

FME HighEFF

Centre for an Energy Efficient and Competitive Industry for the Future



Deliverable D1.2_2020.02

Nonsmooth Analysis for Steady State Simulation of Distillation Processes

Delivery date: 2020-06-15

Organisation name of lead beneficiary for this deliverable:

MIT

HighEFF- Centre for an Energy Efficient and Competitive Industry for the Future is one of Norway's Centre for Environment-friendly Energy Research (FME). Project co-funded by the Research Council of Norway and Industry partners. Host institution is SINTEF Energi AS.		
Dissemination Level		
PU	Public	PU
RE	Restricted to a group specified by the consortium	

Deliverable number:	D1.2_2020.02
ISBN number:	
Deliverable title:	Nonsmooth Analysis for Steady State Simulation of Distillation Processes
Work package:	WP 1.2
Deliverable type:	JP
Lead participant:	MIT

Quality Assurance, status of deliverable		
Action	Performed by	Date
Verified (WP leader)	Sigurd Skogestad	
Reviewed (RA leader)	Egil Skybakmoen	
Approved (dependent on nature of deliverable)*)		

*) *The quality assurance and approval of HighEFF deliverables and publications have to follow the established procedure. The procedure can be found in the HighEFF eRoom in the folder "Administrative > Procedures".*

Authors		
Author(s) Name	Organisation	E-mail address
Suzane M. Cavalcanti	MIT	suzane@mit.edu
Paul I. Barton	MIT	

Abstract
<p>Many process systems, such as distillation columns and other equipment with phase change, exhibit multiple modes of physical behavior that can be described by non-differentiable (i.e., nonsmooth) models. In this paper, we introduce a nonsmooth model for steady-state multistage distillation that can describe columns with dry and/or vaporless stages reliably. The model consists of a system of nonsmooth MESH and specification equations, without inequality or complementarity constraints, that can be directly solved with the semismooth Newton method using automatically computed generalized derivatives. With a modified version of pseudo-arclength continuation, we have been able to observe several novel types of bifurcations in dry and/or vaporless distillation columns. Many of the bifurcations exhibit degenerate behavior with an infinite number of steady states for certain critical input specifications, and occur in general multistage distillation systems regardless of the mixture components or thermodynamic models chosen. We present case studies drawn from the literature and analyze the occurrence and behavior of the bifurcations with respect to several types of column configurations, involving ideal stages, stage efficiencies, pressure gradients, tray heat transfer, multiple feeds, and side products. The associated bifurcation curves are</p>

inherently nonsmooth and can be described mathematically by the concept of piecewise-smooth manifolds introduced in this paper.

Multiple Steady States and Nonsmooth Bifurcations in Dry and Vaporless Distillation Columns

Suzane M. Cavalcanti and Paul I. Barton*



Cite This: *Ind. Eng. Chem. Res.* 2020, 59, 18000–18018

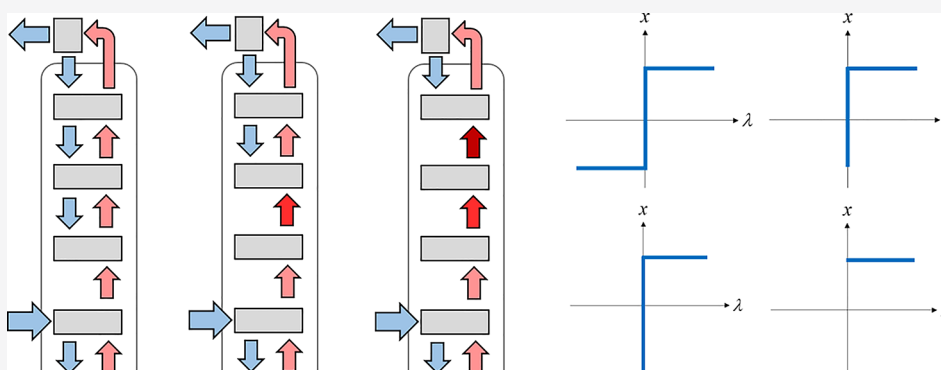


Read Online

ACCESS |

Metrics & More

Article Recommendations



ABSTRACT: Many process systems, such as distillation columns and other equipment with phase change, exhibit multiple modes of physical behavior that can be described by non-differentiable (i.e., nonsmooth) models. In this paper, we introduce a nonsmooth model for steady-state multistage distillation that can describe columns with dry and/or vaporless stages reliably. The model consists of a system of nonsmooth MESH and specification equations, without inequality or complementarity constraints, that can be directly solved with the semismooth Newton method using automatically computed generalized derivatives. With a modified version of pseudo-arclength continuation, we have been able to observe several novel types of bifurcations in dry and/or vaporless distillation columns. Many of the bifurcations exhibit degenerate behavior with an infinite number of steady states for certain critical input specifications, and occur in general multistage distillation systems regardless of the mixture components or thermodynamic models chosen. We present case studies drawn from the literature and analyze the occurrence and behavior of the bifurcations with respect to several types of column configurations, involving ideal stages, stage efficiencies, pressure gradients, tray heat transfer, multiple feeds, and side products. The associated bifurcation curves are inherently nonsmooth and can be described mathematically by the concept of piecewise-smooth manifolds introduced in this paper.

INTRODUCTION

Distillation is the most widely used industrial separation method; however, the large amounts of heat needed to create a second phase for vapor–liquid contact make this unit operation very energy-intensive. Distillation operations are responsible for as much as 30% of the total energy use in the industry¹ and for 90–95% of separation energy.² In order to develop more energy-efficient distillation processes, we need an accurate model that can be solved reliably under all process conditions encountered during column design and flowsheet optimization.

Trayed columns are still prevalent in unit operations for two-phase contact, such as absorption, stripping, and distillation,³ whereas packed column simulation also commonly employs an equivalent number of stages. Though the rate-based modeling approach⁴ describes the complex transport phenomena in multistage columns much more realistically than the efficiency/equilibrium stage approach, the former relies on

empirical correlations for hydrodynamic, heat transfer, and mass transfer parameters, which depend on tray geometry and column configuration.⁵ Therefore, equilibrium stage models are still invaluable for the preliminary stages of process design, when detailed column specifications are not established yet. This simpler modeling approach is also widely used in industrial practice because it requires less computational effort, and condenses all deviations from ideal mass transfer behavior into a single parameter, the stage efficiency.

Received: May 7, 2020
Revised: September 4, 2020
Accepted: September 4, 2020
Published: September 4, 2020



The efficiency/equilibrium stage approach to steady-state simulation of multistage separations employs the MESH (Mass balance, Equilibrium, Summation and energy balance, where H stands for enthalpy) equations, which assume that vapor–liquid equilibrium exists at the conditions of each stage. In the rate-based approach, vapor–liquid equilibrium is also enforced at the phase interface between the bulk vapor and liquid phases. However, certain process specifications can lead to a steady state in which the exiting liquid or vapor phase is absent from one or more stages. In a dry/vaporless stage, the remaining vapor/liquid outlet stream can be superheated/subcooled; under these conditions, vapor–liquid equilibrium no longer exists and consequently both the MESH-equation and rate-based models are no longer valid. This gives rise to the often-experienced “dry column” simulation errors in commercial process software, such as the Aspen Plus⁶ RadFrac multistage column model. For these “problematic” process specifications, it is widely known that RadFrac’s equilibrium-stage model aborts all calculations and exhibits a severe error message stating that stages “dried up” of liquid and/or vapor. In addition, we have found that RadFrac’s rate-based model (previously called RateFrac) also fails to converge and prompts a general error message, without detailing its cause.

One might argue that the absence of a valid model to simulate distillation columns with dry/vaporless stages is irrelevant, since such steady-state solutions correspond to extreme and undesirable operating conditions. However, given a certain set of process specifications, we cannot predict a priori which phases will be present within each stage in the column. When current distillation software is unable to find a vapor–liquid equilibrium solution, the user is left with the complicated task of changing specifications by trial-and-error until the model can converge, which is especially challenging within a flowsheet with several interconnected equipment and recycles. Additionally, process specifications are iteratively changed outside user control in sequential-modular simulation of flowsheets with recycle streams, design specifications, and in process optimization; therefore, the solution algorithms might stray into dry/vaporless conditions and fail to converge.

Without a suitable model, we cannot answer a very fundamental question: what is the steady-state behavior of columns with dry/vaporless stages? In order to obtain these steady states, we must change the model equations that describe each stage to reflect which phases (vapor–liquid, vapor only, or liquid only) are present at the solution; however, we have no knowledge of the latter prior to simulation. It is possible to create a single model that automatically “switches” between describing equations and selects the correct ones, at the cost of introducing nonsmooth (i.e., non-differentiable) behavior and requiring more advanced mathematical tools not present in commercial software.

Previous work on steady-state simulation of dry/vaporless distillation columns, using MESH-based models, dates back to the 1990s and is limited to two other papers.^{7,8} In the first paper,⁷ the equilibrium relationship for each stage is relaxed in dry/vaporless regimes by introducing inequalities in terms of a slack variable. In order to address the inequalities, the original task of simulating the process is transformed into the optimization problem of minimizing the slack variable. In the subsequent work,⁸ the KKT conditions for a similar optimization formulation are used to create a model with complementarity constraints. The latter are rewritten as nonsmooth equations in terms of the max operator, and the

model must be solved iteratively as a series of smooth-approximation problems. However, in both papers, only limited simulation results with dry/vaporless columns are reported, corresponding to very few sets of column specifications. As demonstrated by the present paper, these do not give the full picture of *how* the vapor/liquid “drying” process occurs within the column.

To this date, all other subsequent papers that address modeling of dry/vaporless distillation regimes^{9–14} have considered flowsheet optimization only—the type of problem where complementarities are ostensibly easier to handle mathematically. However, all the aforementioned approaches rely either on a series of equation-solving problems or on optimization algorithms even when only a single simulation is needed. This increases computational effort and introduces nonphysical variables and parameters that need to be heuristically tuned for each process flowsheet.

On the other hand, recent advances in the automatic evaluation of generalized derivatives¹⁵ have opened up the possibility of creating explicitly nonsmooth algebraic models that can be directly solved with Newton-like methods. By introducing a single nonsmooth equation in terms of the mid function, which returns the median of its three arguments, Watson et al.^{16,17} have successfully reformulated the phase equilibrium problem for a single stage in order to perform flash calculations and model multistream heat exchangers with phase change. With an analogous approach, Sahlodin et al.¹⁸ proposed a nonsmooth dynamic model for multistage distillation columns, formulated in terms of liquid and vapor molar holdups.

In this work, we extend the explicitly nonsmooth modeling strategy to steady-state distillation simulation by proposing a nonsmooth MESH model, which remains valid regardless of the phases present in each stage. Using this compact equation-based modeling strategy and by developing a nonsmooth version of the pseudo-arclength continuation method,¹⁹ we have been able to observe infinitely many steady states in distillation columns with dry/vaporless stages. This degenerate behavior occurs for certain critical input specifications independently of the particular mixture being separated or the thermodynamic models used, and persists even when different column configurations are specified.

Bifurcations, or changes in the number of steady-state solutions, have been previously observed in multistage distillation column simulation with smooth models^{20–25} and also confirmed experimentally.^{26,27} Most cases analyzed involve homogeneous azeotropic distillation systems with at least three components,^{20–22} although bifurcations have also been observed in binary distillation²³ and Petlyuk columns.²⁴ In the majority of cases, the curve of steady-state solutions contains two turning points forming a hysteresis curve, and therefore a total number of three steady states exist for parameter values in between the turning points. An extended hysteresis curve, with four turning points yielding up to five steady states, has also been reported within azeotropic distillation.²⁵ In addition, hysteresis behavior is often responsible for the more familiar occurrence of multiple steady states in exothermic chemical reactors. On the other hand, a Hopf bifurcation, with the corresponding appearance of a limit cycle, has also been observed in association with a hysteresis curve for a ternary azeotropic column.²² However, the occurrence of multiple steady states in distillation

simulation might depend, in some instances, on the thermodynamic model used.^{20,28}

Interestingly, Bekiaris et al.²¹ presented the theoretical possibility of infinitely many steady states for homogeneous azeotropic distillation with a simplified analysis, which considered infinite reflux, infinitely many trays, and constant molar overflow. However, to the best of our knowledge, this degeneracy of steady states has not been observed in distillation or other process systems described by more realistic models. Moreover, a distinctive feature of the degenerate bifurcations introduced in this paper is that they involve nonsmooth behavior.

In the following sections, we first discuss the conceptual challenges in describing dry and vaporless equilibrium stages, and present existing nonsmooth modeling strategies and simulation methods. We then describe our nonsmooth MESH model and the numerical continuation strategy developed to trace the curves of infinitely many steady states, while introducing the mathematical concept of piecewise-smooth manifolds that characterize these curves. Next, we conduct detailed parameter continuations in two case studies from the literature^{7,8} and vary several types of column specifications, in order to describe and analyze the degenerate and non-degenerate bifurcations that occur in dry/vaporless distillation columns. Finally, we present a summary of the novel, nonsmooth bifurcations and conclude with remarks on the paper contributions and future lines of work.

■ THE ISSUES WITH DRY AND VAPORLESS STAGES

Consider an equilibrium stage at steady state depicted in Figure 1, which could represent either a flash vessel or, in a

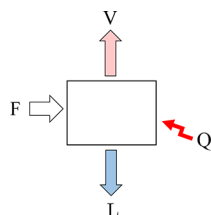


Figure 1. Single-stage flash vessel.

simplified analysis, one of the stages within a column. Let F , L , and V be the total inlet, outlet liquid, and outlet vapor molar flow rates, respectively, and z , x , and y the vectors with mole fractions of the N_c components for each respective stream. The system of MESH equations that models the stage, which assumes that outlet liquid and vapor are in equilibrium, is

$$F = L + V \quad (1)$$

$$Fz_i = Lx_i + Vy_i, \quad i = 1, \dots, N_c \quad (2)$$

$$Fh_F + Q = Lh_L + Vh_V \quad (3)$$

$$y_i = K_i x_i, \quad i = 1, \dots, N_c \quad (4)$$

$$\sum_{i=1}^{N_c} y_i - \sum_{i=1}^{N_c} x_i = 0 \quad (5)$$

where i is the index for a specific component, h_j is the molar enthalpy of stream j , T and P are the stage temperature and pressure, respectively, Q is the heat transfer rate to the stage, and $K_i \equiv K_i(T, P, x, y)$ is the equilibrium ratio for component i .

Note that the single summation equation (eq 5) indirectly enforces both the liquid and vapor phase mole fractions to sum to one, since the mole balances for all the components are included together with the overall mole balance.

Dry and Vaporless Phase Regimes. We define a stage at steady state to be dry if its total outlet liquid flow rate is equal to zero ($L = 0$). Analogously, a stage without a vapor outlet stream is said to be vaporless ($V = 0$). This way, we can characterize the following possible phase regimes for each stage:

- Phase Regime I: a stage with vapor and liquid outlets in equilibrium with each other;
- Phase Regime II: (a) a dry stage with a dew-point vapor outlet and (b) a vaporless stage with a bubble-point liquid outlet;
- Phase Regime III: (a) a dry stage with a superheated vapor outlet and (b) a vaporless stage with a subcooled liquid outlet.

Each set of feasible input parameters, in the correct number to fix the necessary degrees of freedom, may yield a steady state in a certain phase regime. For instance, consider a PT-flash vessel for which all feed conditions are specified. Figure 2

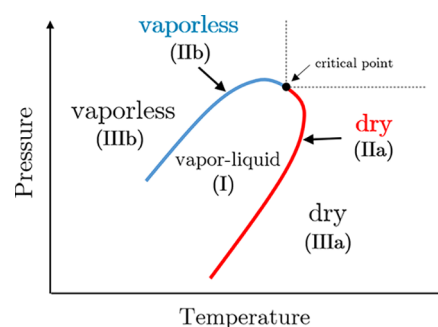


Figure 2. Phase regimes at the solution for each temperature–pressure pair in a PT-flash vessel.

presents a schematic view of the input parameter space in terms of the specified temperature T and pressure P , with the resulting phase regimes at steady state. Note that Phase Regimes II correspond to the nonlinear boundaries between the regions for Phase Regimes I and III.

The MESH Equations Are Not Valid in Phase Regimes III. A robust model must encompass all possible modes of behavior of the system and yield the correct steady state for any set of feasible input specifications. This means that variables characterizing the state of every possible stream in a process, such as compositions and temperatures, must always be included and solved for within the model variables. The mole fractions of an absent liquid or vapor stream are examples of fictitious variables; they bear no physical meaning but can still be computed using the model equations, eqs 1–5, as long as the correlations used to evaluate K_i and the phase enthalpies remain well-defined.

However, suppose that a given set of input specifications leads to a steady state in which the stage operates in Phase Regimes IIIa or IIIb. It can be shown from the KKT conditions for minimization of the Gibbs free energy¹⁸ that, in such a steady state, fictitious mole fractions computed with eq 4 sum to less than one. For instance, for a vaporless steady state with subcooled liquid, $\sum_{i=1}^{N_c} y_i = \sum_{i=1}^{N_c} K_i x_i < 1$. Since the MESH equations (eqs 1–5) always enforce the mole fractions of both

phases to sum to one, they cannot yield the correct steady-state solution. Instead, we obtain a unique but non-physical MESH solution in which the flow rate of the absent phase is negative; in the previous example, $V < 0$. Therefore, the MESH equations are a valid model to describe Phase Regimes I and II but not Phase Regimes III.

Valid Equations for the Dry and Vaporless Phase Regimes. We can propose modified systems of equations to model dry or vaporless stages, both in Phase Regimes II and III, depending on how we formulate and compute the fictitious mole fractions. However, these models are not valid in Phase Regime I (vapor–liquid equilibrium). Any fictitious mole fraction formulation yields the same solutions in terms of physical variables, but the convergence properties of the equation system can be affected by the formulation chosen.

Formulation 1. In this strategy, fictitious mole fractions are computed from the unchanged equilibrium relationship and are not required to sum to one. The system of model equations for a dry stage (Phase Regimes IIa and IIIa) consists of eqs 1–4 and

$$L = 0 \quad (6)$$

which intuitively replaces the summation equation (eq 5). Analogously, the model equations for a vaporless stage (Phase Regimes IIb and IIIb) consist of eqs 1–4 and

$$V = 0 \quad (7)$$

Formulation 2. In this approach, eqs 1–3 and the summation equation (eq 5) are maintained, while the equilibrium relationship in eq 4 is relaxed for all components by introducing a non-physical variable β for each stage:

$$y_i = \beta K_i x_i, \quad i = 1, \dots, N_c \quad (8)$$

This allows the fictitious mole fractions to sum to one but requires an additional model equation to be included: eq 6 for a dry stage and eq 7 for a vaporless stage. Note that, from the previously mentioned result for minimization of the Gibbs free energy, we must have $\beta \leq 1$ for a dry stage and $\beta \geq 1$ for a vaporless stage.

The Phase Regime Cannot Be Predicted Prior to Simulation. Since predicting the exact distribution of regimes within parameter space is a complex task, the mode of behavior corresponding to a given set of input parameters is usually not known before simulating the system. On the other hand, we must choose an equation system and its associated mode of behavior to simulate the process. A naive way to approach this conundrum is by trial-and-error, attempting each system of model equations until one of them converges to a valid solution. While this seems feasible in the case of a single-stage flash, for which only three such models exist, it is not practical for a multistage column. In the latter case, *each stage* has three possible sets of describing equations. The overall number of possible model equations for the column is equal to 3^N , scaling exponentially with the number of stages N . Process simulation software such as Aspen Plus and HYSYS consider only the MESH distillation model, in which all stages are assumed to be in Phase Regime I (vapor–liquid); no dry or vaporless models are included.

Instead, it is possible to create a single model that remains valid in all possible phase regimes, automatically switching between the equations for each stage and enforcing the correct ones without prior knowledge of the regime at the solution. However, this can only be achieved by introducing nonsmooth

or non-differentiable behavior (e.g., the complementarity constraint and explicitly nonsmooth strategies described below) or even discrete variables (e.g., generalized disjunctive programming²⁹).

NONSMOOTH MODELING APPROACHES

Complementarity Constraints. Modeling of equilibrium stages with complementarity constraints is due to Biegler and collaborators.⁸ In their strategy, Formulation 2 is chosen to define fictitious mole fractions. In order to encompass both the dry and vaporless equation systems, other two non-physical slack variables, s_V and s_L , must be added for each stage, aside from β . The overall model consists of eqs 1–3, 5, and 8 and the additional relationships

$$\beta = 1 - s_L + s_V \quad (9)$$

$$0 \leq L \perp s_L \geq 0 \quad (10)$$

$$0 \leq V \perp s_V \geq 0 \quad (11)$$

A complementarity constraint $0 \leq a \perp b \geq 0$ forces at least one of the variables a , b to be zero and both to be non-negative; it can be expressed by the smooth equation $ab = 0$ together with the inequalities $a, b \geq 0$. Equivalently, a complementarity constraint can be reformulated as a single nonsmooth equation that is non-differentiable (at least) at the origin, such as $\min(a, b) = 0$, $a = \max(0, a - b)$, or the Fischer–Burmeister equation $\sqrt{a^2 + b^2} - (a + b) = 0$.

In order to avoid handling inequality constraints within equation solving, Gopal and Biegler⁸ implement distillation simulation with dry and vaporless stages by solving a series of smoothing approximations to the max reformulation $a = \max(0, a - b)$. In subsequent work, Biegler and collaborators^{9,10,12} incorporate the complementarity constraints into nonlinear programs for distillation optimization. The current strategy^{13,14} is to include these constraints in the form of exact penalty terms $\rho \mathbf{a}^T \mathbf{b}$ in the objective function, with the parameter ρ needing to be tuned for each problem at hand. In both simulation and optimization settings, the complementarity constraint approach introduces artificial variables and parameters that need to be tuned, initialized, and updated, and does not allow for simulation with direct equation solving, creating the need to solve a series of problems in addition to the original one. Moreover, the infinitely many steady states described in the present paper have never been obtained or presented within this modeling strategy, perhaps due to difficulties in performing the necessary continuation methods when complementarity constraints are present.

Explicitly Nonsmooth Equations. Non-differentiable functions, such as the absolute value, min and max, can be explicitly used to create a single system of nonsmooth algebraic equations, without inequality constraints, that is a valid model for all system behaviors. This concise approach neither introduces non-physical variables nor increases problem size. As detailed below, recent developments enable us to compute generalized derivatives for these models and to use direct nonsmooth equation-solving methods for process simulation.

In the explicitly nonsmooth model proposed by Watson and Barton,¹⁶ Formulation 1 is used to define the fictitious mole fractions. Equation 5 is replaced with

$$\text{mid}\left(\frac{V}{F}, \sum_{i=1}^{N_c} x_i - \sum_{i=1}^{N_c} y_i, \frac{V}{F} - 1\right) = 0 \quad (12)$$

where the piecewise-smooth function mid returns the median of its three arguments. Equivalently, the third argument can be substituted by $-\frac{L}{F}$. The denominator F in the first and third arguments acts simply as a scaling factor so that all three arguments have a similar order of magnitude, and can therefore be substituted by any other positive constant. With the mid function, we can include three different model equations, respectively eqs 7, 5, and 6, in a single one. The correct expression is automatically satisfied (i.e., becomes the median) according to the phase regime: vaporless ($\frac{V}{F} = 0$), vapor-liquid ($\sum_{i=1}^{N_c} x_i - \sum_{i=1}^{N_c} y_i = 0$), and dry ($\frac{V}{F} - 1 = -\frac{L}{F} = 0$). Equation 12 is potentially nondifferentiable at points where two of the arguments are equal. For instance, in Phase Regimes II, one of the flow rates is zero and the summation relationship in eq 5 is still satisfied. The explicitly nonsmooth approach has been successfully applied to perform flowsheet flash calculations¹⁷ and model multi-stream heat exchangers with¹⁶ and without³⁰ phase change.

The explicitly nonsmooth strategy can also accommodate Formulation 2 with a clear advantage over the complementarity constraint approach, since no slack variables or inequality constraints are introduced. In this case, the system of piecewise-smooth equations consists of eqs 1–3, 5, and 8 and the additional relationship

$$\text{mid}\left(\frac{V}{F}, \beta - 1, \frac{V}{F} - 1\right) = 0 \quad (13)$$

Alternatively, this extra equation associated with the extra variable β in Formulation 2 can be further eliminated by making use of the identity $\beta \equiv \frac{\sum_{i=1}^{N_c} y_i}{\sum_{i=1}^{N_c} K_i x_i}$. One way to do so, as presented by Watson et al.,³¹ is to maintain eqs 1–3 and 5 and replace the N_c equilibrium relationships in eq 4 with

$$y_i \sum_{i=1}^{N_c} K_i x_i = K_i x_i \sum_{i=1}^{N_c} y_i, \quad i = 2, \dots, N_c \quad (14)$$

$$\text{mid}\left(\frac{V}{F}, \sum_{i=1}^{N_c} y_i - \sum_{i=1}^{N_c} K_i x_i, \frac{V}{F} - 1\right) = 0 \quad (15)$$

Watson et al.³¹ recommend choosing the most volatile component to be left out from eq 14 in order to improve numerical conditioning, although any choice of component $i = 1$ is valid.

NONSMOOTH ANALYSIS AND EQUATION SOLVING

Piecewise-Smooth Functions. Nonsmooth models for most chemical engineering processes, including distillation systems as analyzed in the present paper and multistream heat exchangers,¹⁶ can be formulated in terms of piecewise-smooth (PC^∞) functions.

Let r represent either an integer ≥ 1 or ∞ , and C^r denote the class of r -times continuously differentiable functions. According to the definition by Scholtes,³² a vector-valued function $\mathbf{f}: \mathbb{R}^n \rightarrow \mathbb{R}^m$ is said to be PC^r at a point $\mathbf{x}^0 \in \mathbb{R}^n$ if \mathbf{f} is

continuous at \mathbf{x}^0 and there exist an open neighborhood $N(\mathbf{x}^0) \subset \mathbb{R}^n$ and a finite collection of k C^r selection functions $\mathbf{f}_{(i)}: N(\mathbf{x}^0) \rightarrow \mathbb{R}^m$ such that \mathbf{f} is equal to at least one of these functions at each point in this neighborhood; that is

$$\mathbf{f}(\mathbf{x}) = \mathbf{f}_{(i)}(\mathbf{x}) \text{ for some } i \in \{1, \dots, k\}, \quad \forall \mathbf{x} \in N(\mathbf{x}^0) \quad (16)$$

As illustrated in Figure 3, conceptually the domain of \mathbf{f} around \mathbf{x}^0 can be subdivided into regions where \mathbf{f} is equal to a

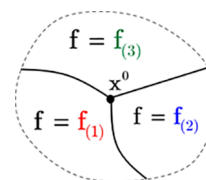


Figure 3. Possible representation of the domain of a PC^r function \mathbf{f} .

C^r selection function $\mathbf{f}_{(i)}$. A function $\mathbf{f}: X \rightarrow \mathbb{R}^m$, with $X \subset \mathbb{R}^n$ open, is said to be PC^r if it is PC^r at every point in its domain X . Since PC^r functions are locally Lipschitz continuous, they can only fail to have a well-defined derivative, represented by the Jacobian matrix $\mathbf{J}\mathbf{f}(\mathbf{x})$, at points \mathbf{x} that belong to a “small” set Z_f (i.e., with Lebesgue measure zero). In Figure 3, Z_f could correspond, at most, to the boundaries between regions.

PC^r functions are closed under composition.³² Examples include the absolute value (abs), maximum (max), minimum (min), and mid operators, which are, in particular, piecewise-smooth (PC^∞).

Generalized Derivatives. A useful generalized derivative for a PC^r function \mathbf{f} is its B-subdifferential $\partial^B \mathbf{f}(\mathbf{x}^0)$ at a point \mathbf{x}^0 , which corresponds to the set of limiting derivatives (Jacobian matrices) as we approach \mathbf{x}^0 :

$$\partial^B \mathbf{f}(\mathbf{x}^0) := \left\{ \lim_{i \rightarrow \infty} \mathbf{J}\mathbf{f}(\mathbf{x}_{(i)}) \text{ such that } \lim_{i \rightarrow \infty} \mathbf{x}_{(i)} = \mathbf{x}^0 \text{ and } \mathbf{x}_{(i)} \notin Z_f \right\} \quad (17)$$

For instance, the B-subdifferential for the absolute value function at the origin contains two elements, -1 and 1 . The algorithm by Khan and Barton¹⁵ provides the first method to obtain exact B-subdifferential elements for PC^r functions, which is based on the concept of lexicographic-directional (LD-)derivatives. Unlike other generalized derivatives, LD-derivatives follow a (strict) chain rule and can be evaluated using automatic differentiation techniques.

The Semismooth Newton Method. To solve the nonlinear system of smooth equations $\mathbf{f}(\mathbf{x}) = 0$ with Newton’s method, we start from a current solution estimate \mathbf{x}^k and generate the next iterate \mathbf{x}^{k+1} by solving the linear system

$$\mathbf{J}\mathbf{f}(\mathbf{x}^k)(\mathbf{x}^{k+1} - \mathbf{x}^k) = -\mathbf{f}(\mathbf{x}^k) \quad (18)$$

The semismooth Newton method³³ naturally extends this to nonsmooth functions by using some adequate generalized derivative element instead of the Jacobian $\mathbf{J}\mathbf{f}(\mathbf{x}^k)$ in eq 18. In particular, when \mathbf{f} is PC^r and a B-subdifferential element is used, the semismooth Newton method achieves the same quadratic convergence rate as the standard Newton method in a neighborhood of a solution \mathbf{x}^* , provided $\partial^B \mathbf{f}(\mathbf{x}^*)$ contains no singular matrices.³⁴

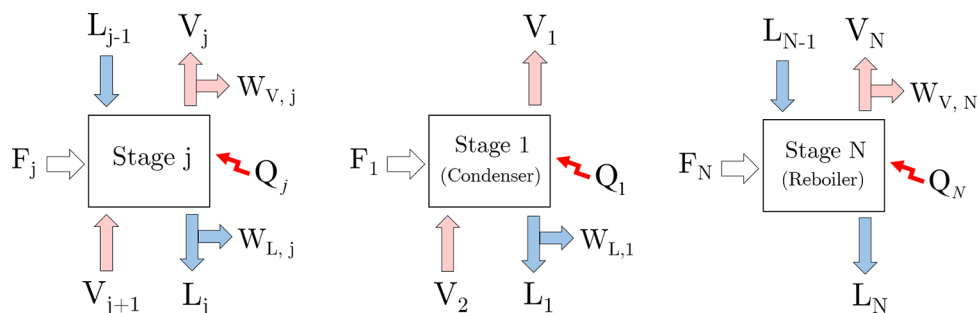


Figure 4. Intermediate stage j (left), the condenser (center), and the reboiler (right) in a distillation column.

■ THE PROPOSED NONSMOOTH MESH MODEL

Consider a steady-state distillation column with N stages, numbered from top to bottom, separating a mixture with N_c components. For each generic stage j , as depicted in Figure 4, we propose a modified system of nonsmooth MESH equations:

$$L_{j-1} + V_{j+1} + F_j - (L_j + W_{L,j}) - (V_j + W_{V,j}) = 0 \quad (19)$$

$$x_{i,j-1}L_{j-1} + y_{i,j+1}V_{j+1} + z_{i,j}F_j - x_{i,j}(L_j + W_{L,j}) - y_{i,j}(V_j + W_{V,j}) = 0, \quad i = 1, \dots, N_c \quad (20)$$

$$h_{j-1}^L L_{j-1} + h_{j+1}^V V_{j+1} + h_j^F F_j - h_j^L (L_j + W_{L,j}) - h_j^V (V_j + W_{V,j}) + Q_j = 0 \quad (21)$$

$$y_{i,j} - K_{i,j}x_{i,j} = 0, \quad i = 1, \dots, N_c \quad (22)$$

$$\text{mid}\left(\frac{V_j + W_{V,j}}{F_s}, \sum_{i=1}^{N_c} x_{i,j} - \sum_{i=1}^{N_c} y_{i,j}, \frac{-(L_j + W_{L,j})}{F_s}\right) = 0 \quad (23)$$

where V_j and L_j are the liquid and vapor molar flow rates leaving stage j , with the respective mole fractions $y_{i,j}$, $x_{i,j}$ of component i ; F_j and $z_{i,j}$ are the molar flow rate and mole fractions of the feed stream to stage j ; $W_{V,j}$ and $W_{L,j}$ are the flow rates of vapor and liquid side products withdrawn from the stage; h_j^V and h_j^L are the molar enthalpies of the outlet vapor and liquid phases; $K_{i,j}$ is the equilibrium ratio for component i ; Q_j is the heat transfer rate to the stage, and F_s is the sum of the feed flow rates to all stages. As illustrated in Figure 4, some of the streams are absent in the first and last stages.

The Mid Equation. Two modifications are introduced into the first and third arguments of the original mid equation (eq 12) for a single-stage flash. First, the numerators of these two arguments, which represent the overall vapor and liquid outlets of the stage, now include the side product stream flow rates $W_{V,j}$ and $W_{L,j}$, respectively. Second, instead of the overall inlet flow rate $L_{j-1} + V_{j+1} + F_j$, particular to each stage j , F_s is used in the denominators as a constant scaling factor for all stages.

Here, we note that the mid equation not only relaxes the summation equation in Phase Regimes III but also automatically bounds the total outlet flow rates $(V_j + W_{V,j})$ and $(L_j + W_{L,j})$ to be non-negative. To see why that is, consider a vaporless stage: in case $(V_j + W_{V,j})$ assumes a negative value, both the first and third arguments of the mid function are strictly negative and therefore the median cannot equal zero to

satisfy the equation. However, unlike the single-stage flash case, the individual flow rates L_j or V_j are not guaranteed to be non-negative at the solution if a liquid or vapor side product is present, respectively.

The above equations employ Formulation 1 to define the fictitious mole fractions, but the other two forms of Formulation 2 can equivalently be used by making the necessary modifications previously described. When using eq 13, one extra variable β_j must be included for each stage.

The Condenser. The total distillate flow rate D is given by

$$D = W_{L,1} + V_1 \quad (24)$$

and the reflux ratio is defined as $R = L_1/D$. The vapor distillate fraction $\theta = V_1/(W_{L,1} + V_1)$ for the condenser, ranging from 0 to 1, must be specified with an additional equation.

For a partial condenser ($0 < \theta \leq 1$), the mid equation (eq 23) is maintained. For a total condenser ($\theta = 0$), since $V_1 = 0$ is constant, the mid equation is replaced with

$$\sum_{i=1}^{N_c} x_{i,1} - y_{i,1} = 0 \quad (25)$$

to ensure a bubble-point outlet liquid stream.

Stage Efficiencies. Equations 19–23 define an ideal stage in which vapor–liquid mass transfer happens to its full extent, with outlet vapor and liquid mole fractions related through the equilibrium relationship in eq 22. Instead, less-than-ideal mass transfer in a real stage j can be approximately described by introducing stage efficiencies $\eta_{i,j}$ for each component i . If $\eta_{i,j}^M$ represents the Murphree vapor phase efficiency, eq 22 is replaced with

$$(y_{i,j} - y_{i,j+1}) - \eta_{i,j}^M (K_{i,j}x_{i,j} - y_{i,j+1}) = 0 \quad (26)$$

If the vaporization efficiency $\eta_{i,j}^V$ is specified instead, eq 22 is replaced with

$$y_{i,j} - \eta_{i,j}^V K_{i,j}x_{i,j} = 0 \quad (27)$$

Side Products. Aside from the main top and bottom products with flow rates D and L_N , respectively, vapor and/or liquid side products can also be withdrawn from intermediate stages ($2 \leq j \leq N - 1$). Most formulations of the MESH equations in the literature are defined in terms of withdrawal ratios, such as $W_{L,j}/L_j$ or $1 + W_{L,j}/L_j$. However, these ratios become undefined for dry or vaporless stages, and therefore it is essential to choose the withdrawal flow rates $W_{V,j}$, $W_{L,j}$ as the variables in our model.

For stages without side products, $W_{L,j}$ and $W_{V,j}$ are set to zero. When a vapor or liquid side product is present at an intermediate stage, a corresponding specification equation

must be included, usually in terms of either the withdrawal ratio or the side product flow rate.

Withdrawal Ratio Specification. In a non-dry stage, a desired value for the withdrawal ratio $R_{L_j} = W_{L_j}/L_j$ can be enforced by adding a specification equation in the form

$$W_{L_j} - R_{L_j}L_j = 0 \quad (28)$$

This way, W_{L_j} is enforced to zero for a dry stage despite the withdrawal ratio itself becoming undefined, which reflects the physical behavior of a splitter valve. An analogous equation is included for a desired vapor withdrawal ratio $R_{V_j} = W_{V_j}/V_j$.

Flow Rate Specification. In order to enforce a desired value $W_{L_j, \text{spec}}$ for the liquid side product flow rate in stage j , the following nonsmooth specification is included:

$$\min(L_j, -|W_{L_j} - W_{L_j, \text{spec}}|) = 0 \quad (29)$$

This equation enforces the specified value for W_{L_j} and simultaneously bounds L_j to be ≥ 0 . An analogous equation is included for a desired vapor side product flow rate $W_{V_j, \text{spec}}$, bounding V_j to be ≥ 0 .

Specifying the Degrees of Freedom. When we specify the number N of stages, all feed stream conditions, all stage pressures, the heat duties for intermediate stages (commonly set to 0), and all side product ratios or flow rates for intermediate stages, two degrees of freedom remain for a distillation column. In the standard MESH model, these are fixed directly by two specification equations. For instance, desired values R_{spec} and D_{spec} for the reflux ratio and distillate flow rate are specified, respectively, by the equations

$$R - R_{\text{spec}} = 0 \quad (30)$$

$$D - D_{\text{spec}} = 0 \quad (31)$$

However, if $0 \leq \theta < 1$, a nonzero liquid distillate flow rate $W_{L,1}$ is present and the condenser equations presented so far cannot guarantee a non-negative reflux flow rate L_1 . To correct that, we must modify one of these two specification equations and create a formulation analogous to eq 29. For instance, the distillate flow rate specification becomes

$$\min(L_1, -|D - D_{\text{spec}}|) = 0 \quad (32)$$

Model Simulation and Parameter Continuation. Our nonsmooth MESH model is valid for all possible combinations of liquid-only, vapor-only, and liquid–vapor phase regimes in each stage. Moreover, the mathematical behavior of the model reflects the physical behavior of the system: all flow rates are automatically enforced to be greater than or equal to zero, and therefore any solution obtained with our model is physically valid in that regard. Another distinctive feature is that infeasible input parameter values are also mathematically infeasible, and in this case the model has no solution.

The total set of n model equations is represented by the nonsmooth nonlinear system

$$\mathbf{f}(\mathbf{x}, \lambda) = \mathbf{0} \quad (33)$$

where $\mathbf{x} \in \mathbb{R}^n$ represents the n model variables that are solved for, $\lambda \in \mathbb{R}$ represents a single input parameter while all other degrees of freedom remain fixed, and $\mathbf{f}: \mathbb{R}^{n+1} \rightarrow \mathbb{R}^n$ is piecewise-smooth (PC^∞).

In this work, we wish to analyze how the steady-state solutions \mathbf{x} change as we vary the parameter λ . Specifically, we

say that a bifurcation occurs at a parameter value λ^* when there is a change in the number of solutions \mathbf{x} for each λ . Many concepts from bifurcation theory for dynamical systems can be applied to analyze this problem; the only caveat is that no dynamic or stability considerations can be made if $\mathbf{x}'(t) \neq \mathbf{f}(\mathbf{x}, \lambda)$, which is the case for the nonsmooth steady-state MESH model. In a differential-algebraic dynamic model for a distillation column, the differential equations express the time derivatives of the molar and enthalpy holdups of each stage, which are not present as variables in steady-state MESH models.

Bifurcations can be identified with continuation methods, which are responsible for the numerical approximation of the solution set

$$M = \{(\mathbf{x}, \lambda) \in \mathbb{R}^{n+1}: \mathbf{f}(\mathbf{x}, \lambda) = \mathbf{0}\} \quad (34)$$

If the limiting partial Jacobians of \mathbf{f} with respect to \mathbf{x} (represented by $\mathbf{J}_{\mathbf{x}}\mathbf{f}_{(i)}(\mathbf{x}, \lambda)$) remain invertible, we can perform a simple parameter continuation, in which we fix λ and solve for \mathbf{x} using the semismooth Newton method. The limiting partial Jacobians, used to compute the Newton step according to eq 18, are obtained exactly with the automatic differentiation algorithm of Khan and Barton.¹⁵

However, if the limiting partial Jacobians with respect to \mathbf{x} become singular, a bifurcation is likely to be present and Newton-type methods fail in solving for \mathbf{x} directly. In such cases, as introduced in this paper, we can employ a nonsmooth version of pseudo-arclength continuation to trace solution points (\mathbf{x}, λ) as long as the solution set remains a 1-dimensional PC^r manifold.

■ PC^r MANIFOLDS

In this section, we extend the Scholtes³² definition of PC^r functions to include cases in which the domain is not an open set in Euclidean space. In turn, this allows us to define the concept of a PC^r homeomorphism in non-necessarily local terms and to propose the concepts of PC^r manifolds and PC^r manifolds with boundary.

Definition 1 (PC^r Homeomorphism). Let $U \subset \mathbb{R}^n$ and $V \subset \mathbb{R}^m$ be arbitrary sets and $\phi: U \rightarrow V$ be a function.

- (1) ϕ is said to be a PC^r function if for every point $\mathbf{x} \in U$ there exists an open neighborhood $N_{\mathbf{x}} \subset \mathbb{R}^n$ of \mathbf{x} and a PC^r function $\hat{\phi}: N_{\mathbf{x}} \rightarrow V$ that coincides with ϕ on the intersection $N_{\mathbf{x}} \cap U$.
- (2) ϕ is said to be a PC^r homeomorphism if it is invertible and both ϕ and its inverse $\phi^{-1}: V \rightarrow U$ are PC^r functions.

Definition 2 (PC^r Manifold). A set $M \subset \mathbb{R}^n$ is called a k -dimensional PC^r manifold if for every point $\mathbf{x} \in M$ there exists an open neighborhood $U \subset M$ of \mathbf{x} , an open subset $V \subset \mathbb{R}^k$, and a PC^r homeomorphism $\phi: U \rightarrow V$.

Definition 3 (PC^r Manifold with Boundary). Let \mathbb{H}^k denote the closed half-space

$$\mathbb{H}^k = \{\mathbf{x} = (x_1, \dots, x_k) \in \mathbb{R}^k: x_k \geq 0\} \quad (35)$$

A set $M \subset \mathbb{R}^n$ is called a k -dimensional PC^r manifold with boundary if for every point $\mathbf{x} \in M$ there exists an open neighborhood $U \subset M$ of \mathbf{x} , an open subset $V \subset \mathbb{H}^k$, and a PC^r homeomorphism $\phi: U \rightarrow V$.

Note that, in Definitions 2 and 3, the neighborhood U of \mathbf{x} is open with respect to the topology of M but usually not open with respect to \mathbb{R}^n , which justifies the need for Definition 1.

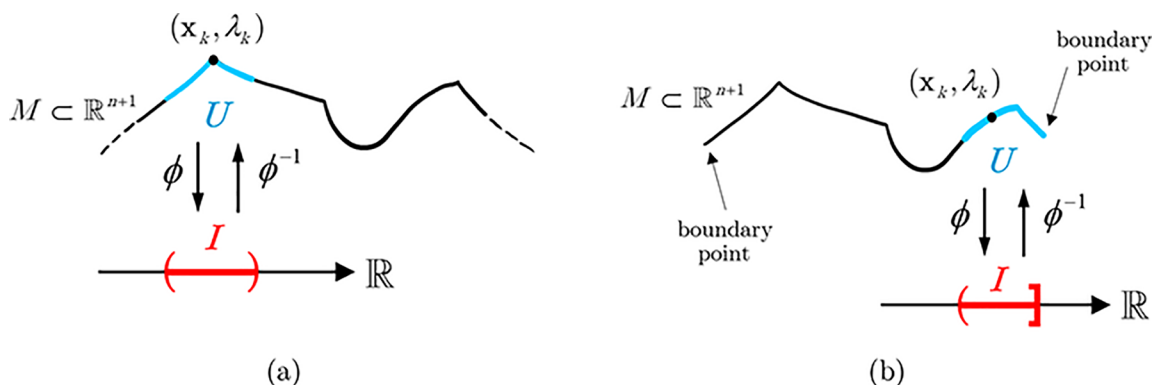


Figure 5. (a) 1-dimensional PC^r manifold. (b) 1-dimensional PC^r manifold with two boundary points.

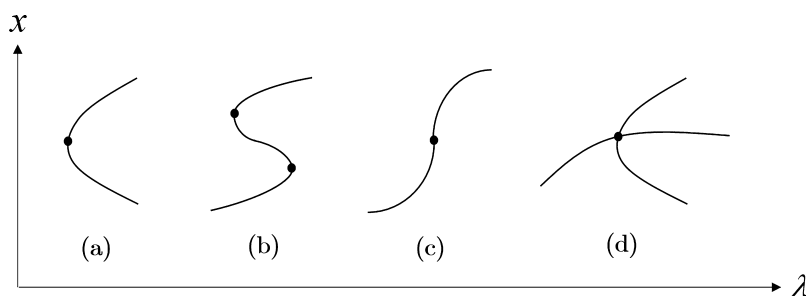


Figure 6. (a) Turning point. (b) Hysteresis curve (two turning points). (c) Hysteresis point. (d) Pitchfork bifurcation point.

Now, suppose the solution set $M \subset \mathbb{R}^{n+1}$ to $f(\mathbf{x}, \lambda) = 0$ is a 1-dimensional PC^r manifold (Figure 5a). This means that, on an open neighborhood $U \subset M$ of every solution point $(\mathbf{x}_k, \lambda_k) \in M$, points in the solution set can be expressed as a function of a single parameter $v \in \mathbb{R}$:

$$(\mathbf{x}, \lambda) = \phi^{-1}(v) \tag{36}$$

where $\phi^{-1}: I \rightarrow U$ is a PC^r homeomorphism and $I \subset \mathbb{R}$ is an open interval. The PC^r functions ϕ^{-1} and ϕ are called a local parametrization and a local coordinate map, respectively. On the other hand, if M is a 1-dimensional PC^r manifold with boundary (Figure 5b), then I might also be a half-closed interval, and any point (\mathbf{x}, λ) corresponding to the closed endpoint of such an interval I is called a boundary point.

■ PSEUDO-ARLENGTH CONTINUATION METHODS

Smooth Systems. The pseudo-arclength continuation method, developed by Keller¹⁹ for smooth functions, can be used to trace the solution set $M \subset \mathbb{R}^{n+1}$ to $f(\mathbf{x}, \lambda) = 0$ when $f: \mathbb{R}^{n+1} \rightarrow \mathbb{R}^n$ is a C^2 function that satisfies the regularity condition, i.e., its Jacobian matrix $\mathbf{Jf}(\mathbf{x}, \lambda) \in \mathbb{R}^{n \times (n+1)}$ is full row rank at every solution point (\mathbf{x}, λ) . When this assumption holds, the solution set M is a 1-dimensional C^2 manifold and constitutes a single solution branch. Examples of such behavior include a turning point (Figure 6a), two turning points forming a hysteresis curve (Figure 6b) and a hysteresis or cusp point (Figure 6c), at which $\mathbf{J}_x f(\mathbf{x}, \lambda)$ is singular but $\mathbf{Jf}(\mathbf{x}, \lambda)$ remains full row rank. In contrast, $\mathbf{Jf}(\mathbf{x}, \lambda)$ is rank-deficient at a pitchfork bifurcation point (Figure 6d), where two solution branches intersect.

Starting from a known solution $(\mathbf{x}_k, \lambda_k)$ of eq 33, the next point $(\mathbf{x}_{k+1}, \lambda_{k+1})$ on the solution branch is obtained in three steps, as schematically illustrated in Figure 7.

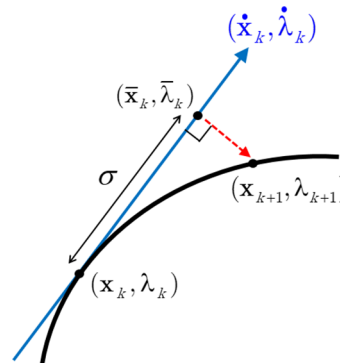


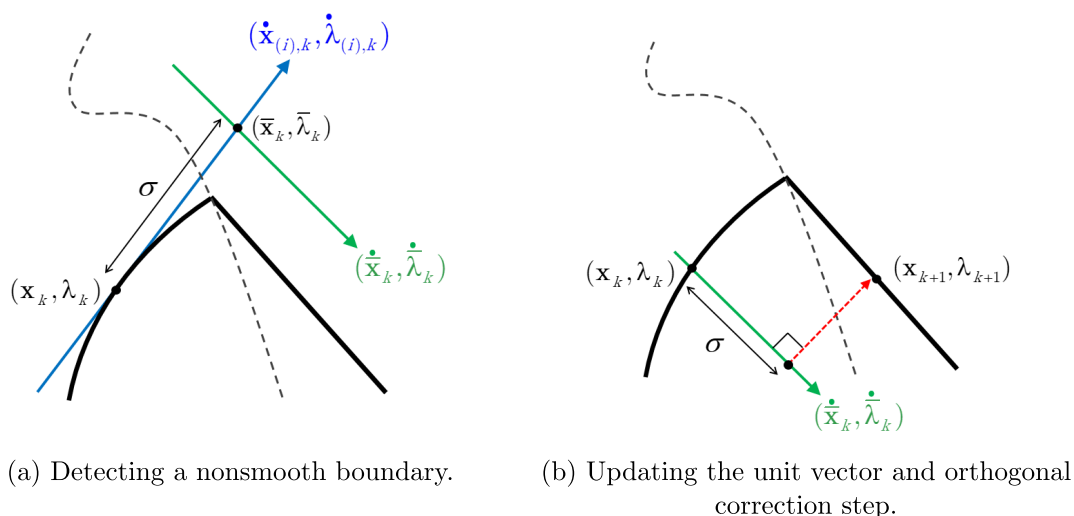
Figure 7. Pseudo-arclength continuation method.

Step 1: Obtain the Unit Tangent Direction. A unit tangent vector $(\hat{\mathbf{x}}_k, \hat{\lambda}_k)$ to the solution branch at $(\mathbf{x}_k, \lambda_k)$ is obtained from the 1-dimensional null space of $\mathbf{Jf}(\mathbf{x}_k, \lambda_k)$. Its direction is chosen such that the continuation process moves in the same direction along the solution branch, which, according to Keller,¹⁹ can be done by enforcing a positive inner dot product between the current and previous tangent vectors:

$$(\hat{\mathbf{x}}_k)^T \hat{\mathbf{x}}_{k-1} + \hat{\lambda}_k \hat{\lambda}_{k-1} > 0 \tag{37}$$

Step 2: Take a Predictive Step along the Tangent Direction. While arc length corresponds to the distance between any two points along the actual solution branch, pseudo-arclength is locally defined with respect to each point $(\mathbf{x}_k, \lambda_k)$ and corresponds to the distance traveled in the tangent direction determined by $(\hat{\mathbf{x}}_k, \hat{\lambda}_k)$. Starting from the current point $(\mathbf{x}_k, \lambda_k)$, we take a pseudo-arclength step of size σ to generate the point

$$(\bar{\mathbf{x}}_k, \bar{\lambda}_k) = (\mathbf{x}_k, \lambda_k) + \sigma(\hat{\mathbf{x}}_k, \hat{\lambda}_k) \tag{38}$$



(a) Detecting a nonsmooth boundary.

(b) Updating the unit vector and orthogonal correction step.

Figure 8. PC^r pseudo-arclength continuation.

which is an initial guess (or an Euler predictor) for the next point on the solution branch.

Step 3: Make an Orthogonal Correction. The next point $(\mathbf{x}_{k+1}, \lambda_{k+1})$ on the solution branch corresponds to the solution of the following augmented nonlinear system:

$$\mathbf{h}(\mathbf{x}, \lambda) = \begin{pmatrix} \mathbf{f}(\mathbf{x}, \lambda) \\ (\dot{\mathbf{x}}_k)^T(\mathbf{x} - \mathbf{x}_k) + \dot{\lambda}_k(\lambda - \lambda_k) - \sigma \end{pmatrix} = \mathbf{0} \quad (39)$$

This system can readily be solved with Newton's method, since its Jacobian matrix

$$\mathbf{Jh}(\mathbf{x}, \lambda) = \begin{pmatrix} \mathbf{Jf}(\mathbf{x}, \lambda) \\ \dot{\mathbf{x}}_k & \dot{\lambda}_k \end{pmatrix} \quad (40)$$

is guaranteed to remain invertible for $\sigma > 0$ small enough, and the predictor point $(\bar{\mathbf{x}}_k, \bar{\lambda}_k)$ is used as the initial guess. The first n equations in eq 39 ensure that the next point lies on the solution manifold within numerical precision, and thus no integration errors are incurred. On the one hand, this allows for an adaptive step size strategy, in which σ can be increased by a suitable percentage whenever the Newton correction converges, and decreased otherwise until convergence is reestablished. On the other hand, in this work we chose instead to trace the solution branch in terms of its actual arc length; this can be achieved by keeping σ small enough so that the distance between consecutive solution points becomes numerically indistinguishable, within a 0.1% relative tolerance, from their pseudo-arclength distance. Finally, the last equation in eq 39 geometrically enforces the next point to belong to a plane that is orthogonal to the tangent direction and situated at an orthogonal distance σ from the current point $(\mathbf{x}_k, \lambda_k)$.

Nonsmooth PC^r Systems. In this work, we extend the pseudo-arclength continuation method to PC^r functions $\mathbf{f}: \mathbb{R}^{n+1} \rightarrow \mathbb{R}^n$ for which the solution set to $\mathbf{f}(\mathbf{x}, \lambda) = \mathbf{0}$ is a 1-dimensional PC^r manifold. This means that the solution branch can only fail to be differentiable at isolated points, for which two distinct limiting tangent directions exist. We further assume that only two distinct limiting Jacobians $\mathbf{Jf}_{(i)}(\mathbf{x}, \lambda)$ can exist at the non-differentiable points; this assumption is satisfied by the nonsmooth MESH model. The modifications introduced into each of the three steps of the smooth pseudo-

arclength method are described below and depicted in Figure 8.

Step 1: Obtain a Limiting Unit Tangent Direction. A limiting Jacobian matrix at the current point, $\mathbf{Jf}_{(i)}(\mathbf{x}_k, \lambda_k)$, is computed exactly with the method of Khan and Barton,¹⁵ and its 1-dimensional null space yields a limiting unit tangent vector $(\dot{\mathbf{x}}_{(i),k}, \dot{\lambda}_{(i),k})$ to the PC^r solution branch at $(\mathbf{x}_k, \lambda_k)$. We have found that requiring a positive dot product between subsequent limiting tangent vectors (eq 37) is not a valid strategy in general to ensure the correct direction, since these pairs of vectors are often orthogonal. Instead, we have resorted to problem-specific information; for instance, for a drying column, the direction is chosen so as to decrease the liquid flow rates in the column.

Step 2: Take a Predictive Step, Detect Nonsmooth Boundaries, and Update the Direction. An Euler predictor step is taken with eq 38 using $(\dot{\mathbf{x}}_{(i),k}, \dot{\lambda}_{(i),k})$, and the active selection function for the PC^r equation system is monitored. If the latter function changes, we know that the method has crossed a nonsmooth boundary in the domain of \mathbf{f} . We have found that convergence of Step 3 is unlikely in this case, since the orthogonal hyperplane corresponding to the limiting tangent direction on one side of the boundary might not intersect the solution branch on the other side. To address this problem in our case studies with the nonsmooth MESH model, we compute a limiting Jacobian matrix $\mathbf{Jf}_{(j)}(\bar{\mathbf{x}}_k, \bar{\lambda}_k)$ at the predictor point. Its null space yields an updated unit vector $(\dot{\mathbf{x}}_{(j),k}, \dot{\lambda}_{(j),k})$ (Figure 8a) that substitutes $(\dot{\mathbf{x}}_{(i),k}, \dot{\lambda}_{(i),k})$ and provides a different orthogonal hyperplane, which we have found to be more likely to intercept the solution manifold. The Euler predictor step is recomputed,¹ and we proceed to Step 3 with the updated unit vector $(\dot{\mathbf{x}}_{(j),k}, \dot{\lambda}_{(j),k})$ (Figure 8b).

Step 3: Make a Nonsmooth Orthogonal Correction. The augmented nonlinear system in eq 39, which is now PC^r , is solved with the semismooth Newton method to generate the next point $(\mathbf{x}_{k+1}, \lambda_{k+1})$.

■ BIFURCATIONS IN DRY/VAPORLESS DISTILLATION COLUMNS

In this section, we present detailed parameter continuations for the two case studies previously considered in the relevant literature^{7,8} and describe new types of bifurcations observed in dry and/or vaporless multistage distillation columns, in light of

the proposed concept of PC^r manifolds. Several of these nonsmooth bifurcations exhibit degenerate behavior, with the occurrence of infinitely many steady-state solutions at certain input parameter values.

Case Study 1: Ideal Binary Mixture. A bubble-point liquid stream with 70% benzene, 30% toluene (% mol) is fed to Stage 6 of a column with $N = 27$ ideal stages, and the vapor and liquid phases are described by ideal thermodynamics (Raoult's Law). The intermediate stages are adiabatic, and a linear pressure profile is specified, ranging from the total condenser (Stage 1) at 1.05 bar to the reboiler (Stage N) at 1.2 bar. The distillate-to-feed ratio is fixed at $D/F = 0.5$, and the feed flow rate is chosen as $F = 100$ mol/s. The only change made to the original case study^{7,8} is that we have switched the feed from Stage 20 to 6 to create clearer plots and illustrations of the drying process. For all case studies in this paper, parameters for the K value and phase enthalpy correlations are retrieved from the Aspen Plus V10 database.⁶ The nonsmooth model equations, and the nonsmooth equation-solving and pseudo-arclength continuation methods previously described were implemented in Matlab.

We fix the remaining degree of freedom in this system by specifying the reflux ratio R , which represents a single parameter λ on which the nonsmooth MESH model equations (represented by eq 33) depend. Figure 9 illustrates how the

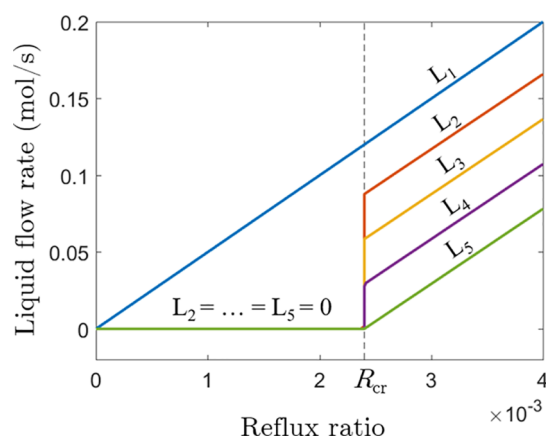


Figure 9. Above-feed liquid flow rates as functions of the reflux ratio R .

steady-state solutions of the model vary as functions of R , in terms of the liquid flow rates coming out of the stages above the feed. When the value of R is high enough, all stages operate with vapor–liquid equilibrium (Phase Regime I); therefore, the original and nonsmooth MESH models have the same unique solution, which varies smoothly with respect to R .

In general, decreasing the reflux ratio causes the vapor and liquid flow rates throughout the column to diminish. The value of R at which one or more flow rates first become zero is denoted here as the critical reflux ratio R_{cr} . Similarly, we can define the critical value λ_{cr} for a general parameter λ . We avoid the “minimum reflux ratio” nomenclature used by Bullard and Biegler⁷ because, as evidenced by Figure 9, it might be possible for the column to operate below R_{cr} while still satisfying all process specifications. Moreover, this phenomenon is not to be confused with the Underwood concept of the minimum reflux ratio to perform a separation, which corresponds to infinitely many stages.

For this particular case study, it is the liquid flow rate L_5 directly above the feed stage that disappears as we approach the critical reflux ratio $R_{cr} \approx 0.0024$ from above. We call the system state corresponding to $R \rightarrow R_{cr}^+$ the *upper critical solution*. In this state, Stage 5 is the only dry stage but it still operates in Phase Regime IIa, and thus the standard MESH equations are still satisfied. However, the MESH model yields a unique but non-physical solution for $R < R_{cr}$, with the above-feed liquid flow rates assuming negative values. On the other hand, the nonsmooth MESH model remains physically valid and reveals an unexpected behavior at R_{cr} , where a continuum of infinitely many steady states exist instead of a unique solution. This is evidenced by the vertical lines in the graphs of L_2 , L_3 , and L_4 at R_{cr} in Figure 9. For this reason, the overall model solution is discontinuous with respect to the reflux ratio at R_{cr} : the *lower critical solution* corresponding to $R \rightarrow R_{cr}^-$ is different from the upper critical solution ($R \rightarrow R_{cr}^+$).

The non-uniqueness of solutions at R_{cr} gives rise to singular limiting partial Jacobians of the model equations $f(\mathbf{x}, R) = \mathbf{0}$ with respect to \mathbf{x} , and therefore the semismooth Newton method fails at or near R_{cr} . In order to obtain these infinitely many steady states, which range from the lower to the upper critical solutions, we had to develop the previously described nonsmooth version of the pseudo-arclength continuation method. By taking small enough continuation steps, we can trace the solutions in terms of arc length as a substitute parameter, which corresponds to the distance traveled along the solution curve in (\mathbf{x}, R) space. Geometrically, arc length acts as an extra coordinate that allows us to “move” perpendicularly to the paper at the vertical line $R = R_{cr}$. Moreover, since a unique steady-state solution exists at each value of arc length, the latter constitutes a more adequate parameter than R to describe the overall set of solutions.

Figure 10 portrays the complete curve of solutions in terms of its arc length starting from $R = 0$, with the corresponding values of reflux ratio represented by the juxtaposed R axis. The vertical line $R = R_{cr}$ from Figure 9 is expanded horizontally in terms of arc length in Figure 10 to reveal an overall solution curve that is continuous but non-differentiable at several points (and including) the upper and lower critical solutions. The state of the distillation column is schematically represented in Figure 10 for all the nonsmooth points, which correspond to when each stage first becomes dry.

Exactly at the upper critical solution ($R \rightarrow R_{cr}^+$), Stage 5 is dry in Phase Regime IIa and V_5 is a dew-point vapor. As we continue tracing the solutions toward smaller values of arc length, L_4 starts decreasing in the same amount that V_5 increases, keeping Stage 5 in mass balance. Concurrently, T_5 increases and makes the vapor V_5 progressively more superheated, putting Stage 5 into Phase Regime IIIa. This is a completely local process, in which only the variables directly associated with Stage 5 change. When L_4 finally reaches zero, we arrive at the next nonsmooth point represented in Figure 10, and further decreasing of arc length initiates this same local process around Stage 4. This way, as we traverse the solutions from $R \rightarrow R_{cr}^+$ to $R \rightarrow R_{cr}^-$, the above-feed Stages 2–5 become dry one at a time, sequentially from bottom to top. For $R < R_{cr}$, decreasing the reflux ratio leads to smaller values of L_1 until the latter reaches zero at $R = 0$. However, the condenser does not become dry because of the specified liquid distillate output $W_{L,1}$. Darker shades of red in Figure 10 represent the degree of “supersaturation” of the vapor streams, which increases as we go up the column due to the pressure drop in each stage.

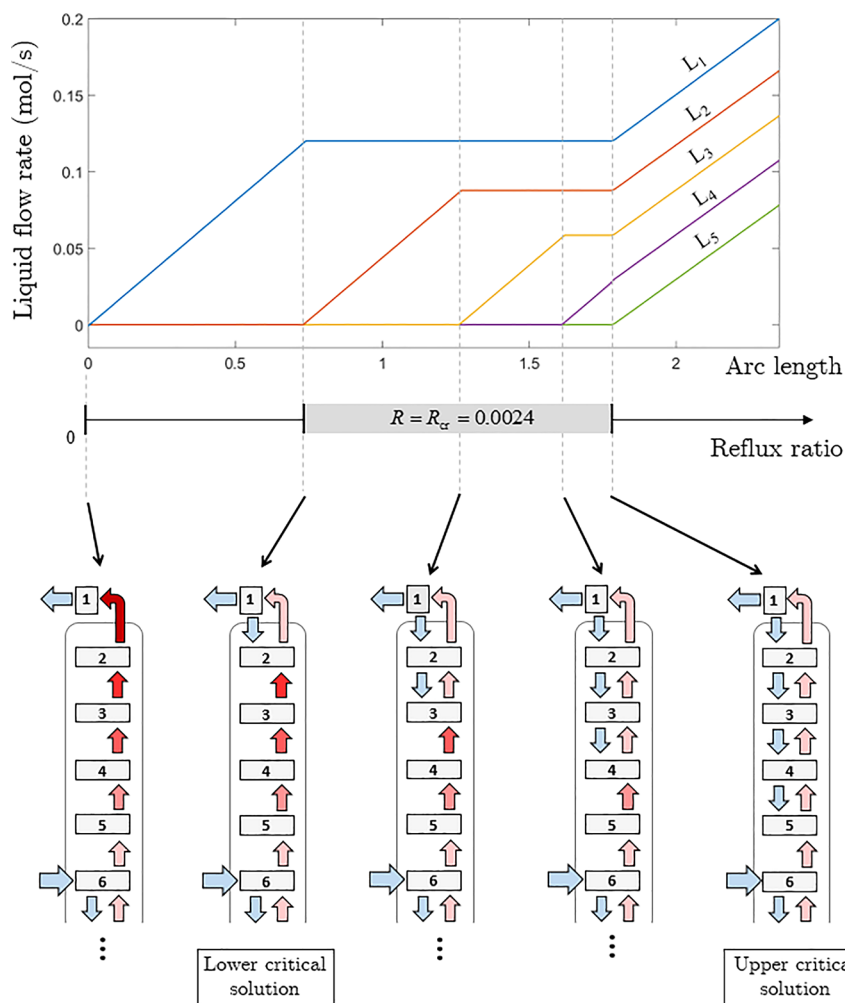


Figure 10. Above-feed liquid flow rates as functions of the arc length of the solution curve, with schematic representations of the column at non-differentiable points.

For negative values of the reflux ratio ($R < 0$), the standard MESH model continues to have a unique mathematical solution, which is nevertheless not physically valid because $L_1 = RD$ and several other liquid flow rates become negative. On the other hand, the nonsmooth MESH model has no mathematical solution for $R < 0$ since its equations bound L_1 to be non-negative, and therefore reflects the behavior of the physical system.

The Bifurcations at $R = R_{cr}$ and $R = 0$. Recall the representation in eq 33 of the nonsmooth MESH model equations as depending on a single parameter λ , which here corresponds to R . We can say that a $1 - \infty - 1$ bifurcation exists at R_{cr} , since the number of model solutions for each value of R changes from 1 for $R < R_{cr}$ to infinitely many at $R = R_{cr}$ and back to 1 for $R > R_{cr}$. Similarly, we observe a $0 - 1 - 1$ bifurcation at $R = 0$, where the solution branch ends abruptly. We can represent the essential aspects of both of these bifurcations in Figure 11 by plotting just the liquid flow rate L_4 against R . However, the behavior of the overall solution set cannot be represented by every one of the variables; for instance, the graph of L_5 does not reveal the occurrence of the bifurcation at R_{cr} . Moreover, note that the intermediate nonsmooth points between the upper and lower critical solutions cannot be observed in terms of L_4 only in Figure 11.

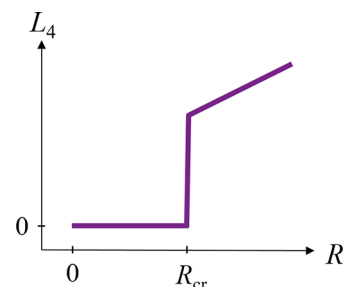


Figure 11. The $0 - 1 - 1$ and $1 - \infty - 1$ bifurcations at $R = 0$ and $R = R_{cr}$, respectively, in terms of L_4 .

We can also observe a bifurcation of type $1 - \infty - 1$ in very simple smooth systems. For instance, for $f(x, \lambda) = \lambda x = 0$, there is a unique solution $x = 0$ for $\lambda \neq 0$, but the whole real line $x = \mathbb{R}$ of solutions at $\lambda^* = 0$. What makes the bifurcation at $R = R_{cr}$ unique and novel is that the overall solution set remains a 1-dimensional and connected PC^r manifold, as illustrated in Figure 11. Moreover, the set of infinitely many solutions at R_{cr} is bounded and, in this case, consists of a 1-dimensional and connected PC^r manifold with two boundary points: the upper and lower critical solutions. Intuitively, this type of bifurcation can be thought of as a *hysteresis region*: a hysteresis point (Figure 6c) that has been “stretched” vertically into a whole

segment of constant $R = R_{cr}$. Note how this differs from the smooth hysteresis curve (Figure 6b) observed in most other distillation systems with bifurcations, which are modeled with the (smooth) MESH equations.

Mathematically, for each of the infinitely many solutions at $R = R_{cr}$, at least one of the limiting partial Jacobian matrices $J_{\mathbf{x}}\mathbf{f}_{(i)}(\mathbf{x}, R_{cr})$ with respect to the variables \mathbf{x} is singular, with a rank 1 deficiency. For the nonsmooth MESH model of a distillation column, these singularities arise from complex interactions between the model equations of types M, E, S, and H of several stages. Intuitively, the singularities are associated with an extra degree of freedom for the model equations, which appears only at R_{cr} and makes the system momentarily underdetermined.

On the other hand, the limiting partial Jacobian matrices $J_{\mathbf{x}}\mathbf{f}_{(i)}(\mathbf{x}, R)$ at $R = 0$ remain invertible despite the occurrence of a bifurcation, and therefore the semismooth Newton method can be used to solve for \mathbf{x} directly at or around $R = 0$. In this case, singular matrices are only present in the Clarke Jacobian set of \mathbf{f} , which corresponds to the set of all convex combinations of the limiting Jacobian matrices $J_{\mathbf{x}}\mathbf{f}_{(i)}(\mathbf{x}, 0)$.

The Choice of Parameter and the Bifurcation at $B = B_{cr}$. We can analyze how the solutions of the nonsmooth MESH model change with respect to any other parameter λ . If we choose to specify and vary the boilup ratio $B = V_N/L_N$ instead of R , we also arrive at a critical boilup ratio B_{cr} at which the first flow rate in the column becomes zero. Figure 12 presents the

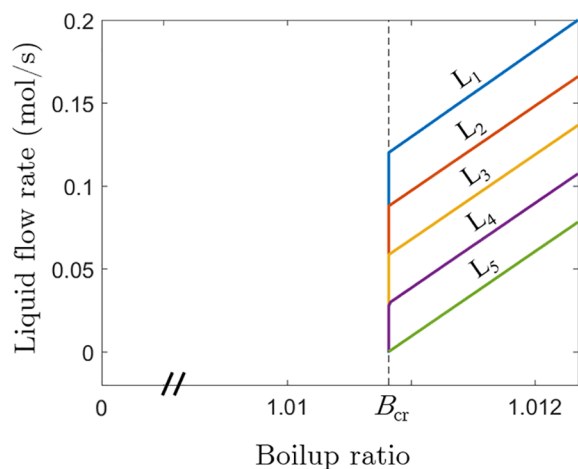


Figure 12. Above-feed liquid flow rates as functions of the boilup ratio B .

above-feed liquid flow rates for Case Study 1 in terms of B , with $B_{cr} \approx 1.0108$. Even though the overall solution set remains the same, its representation in terms of B gives rise to a different bifurcation at B_{cr} of type $0 - / \infty - 1$; here, $/ \infty$ indicates that the set of infinitely many solutions at the bifurcation parameter B_{cr} is bounded and ends abruptly on one end. The upper critical solution solution ($R \rightarrow R_{cr}^+$) now corresponds to $B \rightarrow B_{cr}^+$, and the solution for $R = 0$ would correspond to approaching B_{cr} from below. The essential aspects of this bifurcation can be described by the graph of L_4 versus B in Figure 13; the solution set at B_{cr} is bounded and consists of a 1-dimensional PC^r manifold with two boundary points.

Since no solutions exist below the critical boilup ratio, B_{cr} represents a positive lower bound for the parameter that

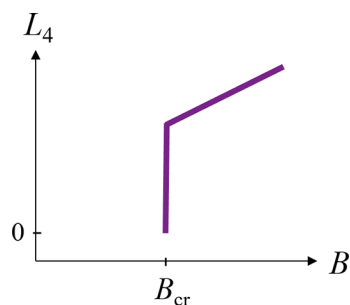


Figure 13. The $0 - / \infty - 1$ bifurcation at B_{cr} in terms of L_4 .

cannot be predicted prior to simulation. This happens because, once L_5 becomes zero at the upper critical solution, the distillation column is split into two halves (Stages 1–4 and Stages 5–27). Changes in the upper half, such as decreases in the value of R , can no longer impact the lower half, whose describing variables (including $B = B_{cr}$) remain the same for $0 \leq R \leq R_{cr}$.

Vapor Feed. Now, consider the same specifications in Case Study 1 except that the feed stream is a dew-point vapor, directly introduced into Stage 6. Figure 14 presents some of the vapor flow rates in the below-feed column section as functions of either R or B . In this case, it is the vapor phase that disappears, but only in the stages below the feed. We can observe a behavior that is mostly analogous to the dry column case, except that the roles of R and B are switched; the critical points for this system are $R_{cr} \approx 1.054$ and $B_{cr} \approx 0.0195$. The below-feed stages become sequentially vaporless from top to bottom, starting with $V_7 = 0$ at $B \rightarrow B_{cr}^+$, then $V_{26} = 0$ at $B \rightarrow B_{cr}^-$ and finally with the reboiler “turning off” and becoming vaporless ($V_{27} = 0$) at $B \rightarrow 0^+$. However, the solution curve behavior at $B = 0$ for a vaporless column is qualitatively different than that of a dry column at $R = 0$.

No solutions exist for $B < 0$ since the mid equation (eq 23) for the reboiler ensures $V_N > 0$. However, at $B = 0$, the reboiler is vaporless and thus the liquid bottoms product L_N is mathematically allowed to become subcooled. This generates infinitely many solutions associated with a negative reboiler heat duty Q_N and gives rise to a $0 - \infty - 1$ bifurcation both at $B = 0$ and at $R = R_{cr}$. This type of bifurcation differs from the $0 - / \infty - 1$ bifurcation depicted in Figure 13 because the solution set is now unbounded at the bifurcation parameter, and consists of a connected 1-dimensional PC^r manifold with a single boundary point (the upper critical solution). The essential aspects of the $0 - \infty - 1$ bifurcations at $B = 0$ and at $R = R_{cr}$ can only be represented in terms of some of the reboiler variables, such as the graph of the reboiler temperature T_N versus the boilup ratio B at $B = 0$ in Figure 15.

Note that a negative reboiler heat duty is physically realizable in terms of heat exchange. However, we can choose to eliminate these infinitely many solutions mathematically by bounding Q_N to be positive, which can be attained by employing a nonsmooth equation analogous to eq 32.

Case Study 2: Five-Component Non-ideal Mixture. A bubble-point liquid stream composed of 15% methanol, 40% acetone, 5% methyl acetate, 20% benzene, and 20% chloroform (% mol) is fed to Stage 7 of a column with $N = 19$ ideal stages. The UNIQUAC activity model is used for the liquid phase, and the Hayden–O’Connell correlation is used to compute the second virial coefficients that model the vapor phase fugacity. The feed-to-distillate ratio is fixed at $D/F = 0.3$, the

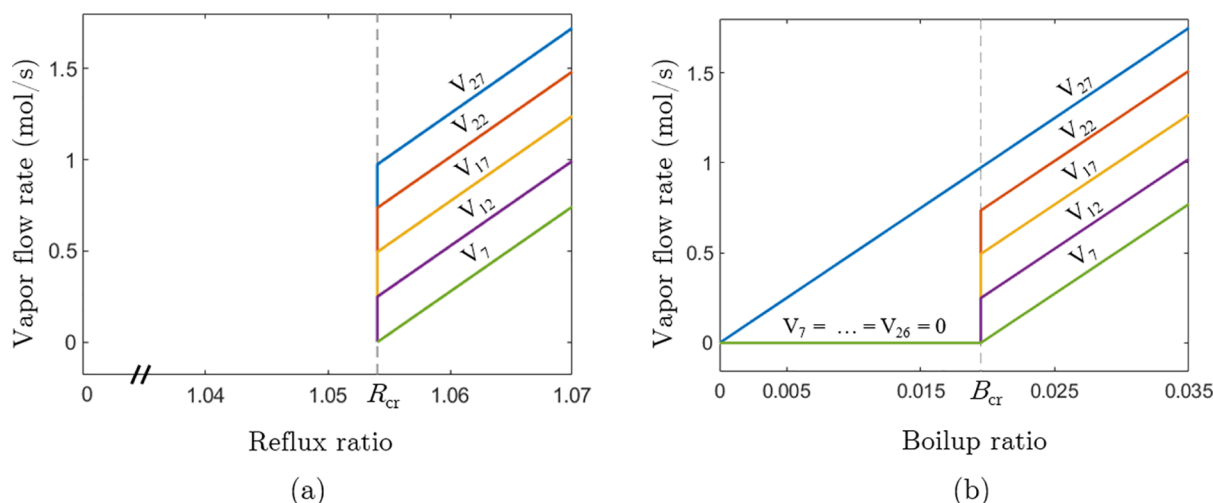


Figure 14. Below-feed vapor flow rates as functions of (a) the reflux ratio R and (b) the boilup ratio B .

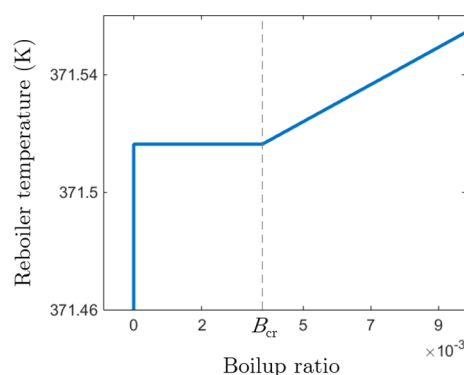


Figure 15. Reboiler temperature T_N as a function of the boilup ratio B .

intermediate stages are adiabatic, and the linear pressure profile ranges from 1.1 bar at the reboiler to 1.015 bar at the total condenser. This system was also considered in the same papers previously mentioned.^{7,8}

Due to its low feed concentration, methyl acetate reaches very small vapor phase mole fractions in the above-feed stages, to the point that its fictitious liquid mole fractions defined via Formulation 1 (eqs 22 and 23) would have to be negative in the dry stages. This precludes convergence of the model equations since the K value correlations contain logarithmic terms that would become undefined. Instead, Formulation 2 can be used to trace all model solutions, with the variable β present either explicitly through eq 13 (Formulation 2a) or implicitly through eqs 14 and 15 (Formulation 2b). In both cases, it is β that changes to reflect deviations from liquid–vapor equilibrium, with the fictitious liquid mole fractions remaining approximately constant. We note that convergence with Formulation 2a is much more robust, which comes at the price of adding an extra β_j variable to each stage j . Formulation 2b can become numerically unstable depending on the component chosen as $i = 1$ in eq 14, including when the most volatile component (acetone) is chosen, and thus smaller continuation steps must be used.

Using either form of Formulation 2, we can observe the same qualitative behavior in this five-component system as seen in the binary Case Study 1, with stages becoming dry (for a liquid feed) or vaporless (for a vapor feed) through the same

previously detailed bifurcations. Therefore, for the sake of brevity, we omit the plots and report only the critical parameter values: $R_{cr} \approx 0.0013$ and $B_{cr} \approx 0.4382$ when the feed is a bubble-point liquid, and $R_{cr} \approx 2.2976$ and $B_{cr} \approx 0.0068$ when the feed is a dew-point vapor.

ANALYSIS OF THE BIFURCATIONS

The bifurcations that occur at the critical parameter values represent the transition of some of the column stages from Phase Regime I (vapor–liquid) into Phase Regimes III (superheated vapor or subcooled liquid), and are intrinsic to cascades of equilibrium stages. In this section, we use the original Case Study 1 (with a liquid feed) as a basis for comparison and introduce several modifications into the column configuration and types of specifications, in order to analyze which factors can influence and give rise to these bifurcations.

Type of Modeling Approach. Any modeling approach capable of enforcing the necessary MESH-based physical laws, with equilibrium relationships only between the phases that are actually present, will invariably lead to the same steady-state solutions and bifurcations described in this paper. In this sense, all three different formulations using the explicitly nonsmooth, PC^∞ function mid that we have employed (eqs 12, 13, and 14, 15) are equally valid. Equivalently, we could have used the complementarity constraint modeling approach represented by eqs 9–11 by first rewriting them with explicitly nonsmooth equations (e.g. the Fischer–Burmeister formulation), and then employing our pseudo-arclength continuation method to yield the same steady-state solutions. However, this approach would be more costly, given that it includes the additional variables s_V , s_L , and β for each stage.

The Critical Parameter Value. The critical parameter value λ_{cr} is particular to each system and cannot be predicted or computed with the MESH equations in general, since the location of the first flow rate(s) to equal zero cannot be predicted. However, λ_{cr} and the upper critical solution can be readily computed by replacing the specification equation for the parameter in the standard MESH model:

$$\lambda - \lambda_{user} = 0 \quad (41)$$

with the explicitly nonsmooth equation

$$\min \left(\min_j L_j, \min_j V_j \right) = 0 \quad (42)$$

Mixture Components and Thermodynamic Models.

Our numerical experiments have shown that all bifurcations presented in this paper are independent of the number and identity of components and the thermodynamic model used, which was also illustrated by Case Study 2. For instance, employing the Peng–Robinson equation of state in the original Case Study 1 maintains the same bifurcation behaviors, while the critical parameter values change slightly ($R_{cr} \approx 0.0023$, $B_{cr} \approx 1.007$). The only issue to consider, as discussed in Case Study 2, is that certain fictitious mole fraction formulations might preclude convergence of the model equations at or below the critical parameter value, depending on the mixture.

Pressure Gradients and Tray Heat Loss. Mathematically, the degenerate bifurcations at the critical parameter values will only occur if “external driving forces” are included in the column specifications, in the form of a pressure gradient and/or external heat transfer in the trays (i.e., intermediate stages). Without at least one of these imposing forces, the vapor and liquid streams cannot drive themselves out of saturation and thus the column stages cannot reach Phase Regimes III. In such cases, there is a unique solution at the critical parameter value, corresponding to when one or more stages first become dry/vaporless but remain in Phase Regimes II.

To demonstrate that, consider Case Study 1, now with a uniform column pressure of 1 bar. As Figure 16 illustrates, the

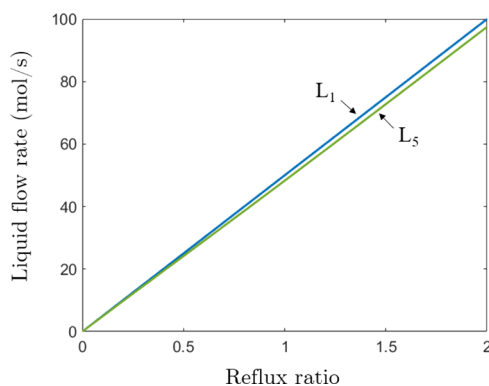


Figure 16. Liquid flow rates L_1 and L_5 versus R for Case Study 1 with a uniform column pressure of 1 bar.

stages above the feed can only become dry simultaneously, with a unique critical solution at $R = R_{cr} = 0$. In terms of the boilup ratio, this unique solution corresponds to $B_{cr} \approx 0.986$. Further decreasing of either R or B would necessarily lead to negative liquid flow rates, which is not allowed by the nonsmooth MESH model; as a result, we have a 0 - 1 - 1 bifurcation both at R_{cr} and B_{cr} .

On the other hand, we can specify a uniform column pressure and still observe the same 1 - ∞ - 1 and 0 - $-\infty$ - 1 bifurcations at R_{cr} and B_{cr} , respectively, by including non-zero tray heat duties Q_j . If we impose a uniform column pressure of 1 bar and include a heat gain $Q_j \approx 9.6 \times 10^2$ J/s in all trays ($2 \leq j \leq N - 1$) in Case Study 1, we are able to reproduce essentially the same solutions and corresponding bifurcations of the original case study, with the same R_{cr} , B_{cr} values. In the case of a vapor feed, the original bifurcations with vaporless

stages are recovered by imposing an external heat loss in the trays.

In a real distillation column, a significant fraction of the tray pressure drop is due to vapor flow through tray perforations. Therefore, we can expect a pressure gradient to be present in dry stages, creating the mathematical conditions for the occurrence of infinitely many steady states with superheated vapor streams at the critical parameter values. Additionally, tray columns are not perfectly insulated and heat exchange with the environment occurs at every stage. In above-ambient-temperature processes, tray heat losses could allow the liquid in vaporless stages to become subcooled, providing the necessary conditions for infinitely many vaporless states to be observed.

Stage Efficiencies. All numerical examples presented thus far involve ideal stages. If, instead, we specify a vaporization efficiency of 30% in all intermediate stages in Case Study 1, we still observe the same bifurcations previously presented, only at different critical parameter values ($R_{cr} \approx 0.00308$, $B_{cr} \approx 2.000$). On the other hand, if we specify vapor-phase Murphree tray efficiencies of 30%, we obtain the slightly different behavior depicted in Figure 17. In this case, mathematically there exists

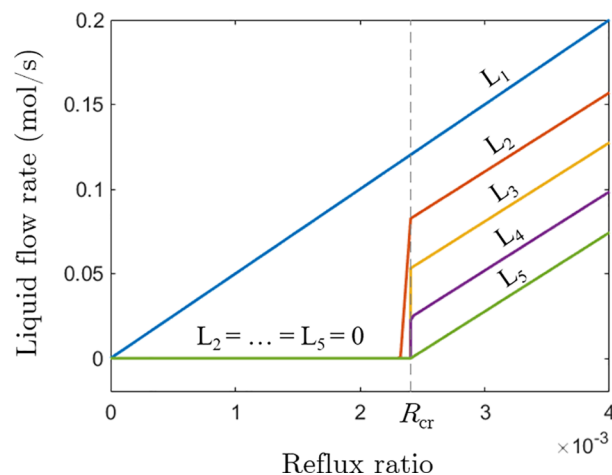


Figure 17. Above-feed liquid flow rates versus R for Case Study 1 with vapor-phase Murphree efficiencies of 30%.

a unique solution for each value of R and therefore no bifurcation is present at $R_{cr} \approx 0.0024$. However, the limiting partial Jacobian matrices $\mathbf{J}_{\mathbf{x}} \mathbf{f}_{(i)}(\mathbf{x}, R)$ become extremely ill-conditioned, despite being non-singular, and the resulting behavior in Figure 17 remains essentially the same. We observe an extremely abrupt change in steady states at R_{cr} with graphs that still appear to be vertical. Finally, we note that the numerical values chosen for the tray efficiencies (either of the vaporization or Murphree types) do not change the types of behaviors observed. The difference in results depending on the type of efficiency chosen suggests that the functional form of the equilibrium relationship (eq 22), maintained when using vaporization efficiencies, is necessary for the mathematical existence of infinitely many solutions.

Notwithstanding, we must take into account that stage efficiencies are only simplified descriptions of non-ideal vapor–liquid mass transfer in real stages, with shortcomings that become more pronounced in multicomponent, non-ideal mixtures.³ Moreover, Murphree stage efficiencies are known to become undefined and/or physically incorrect in several

instances, while vaporization efficiencies can be shown to, at least, always remain well-defined.³⁵ For these reasons, column simulation in distillation design is customarily performed with ideal stages, with stage efficiencies being estimated and included post-simulation only to yield an updated number of trays. In contrast, the non-equilibrium or rate-based modeling strategy is much better suited to describe mass transfer effects in real stages, and thus a nonsmooth version thereof could be more reliable in predicting the steady-state behavior of dry/vaporless columns.

However, the rate-based approach relies on correlations for mass and heat transfer, interfacial areas, and other parameters, which depend on knowledge of column and tray design details,⁵ and are expected to be valid only when both vapor and liquid phases are present. On the other hand, in general, the efficiency/equilibrium stage approach still remains quite accurate to describe binary, close-boiling ideal mixtures,³ such as the benzene–toluene system from Case Study 1. As demonstrated in this section, the fact that the infinitely many steady-state solutions of the nonsmooth MESH model persist under different types of column specifications, stage efficiencies, mixture components, and thermodynamic models at least supports the hypothesis that some type of degenerate or near-degenerate behavior could be observed experimentally.

The Feed State. It is the state of the feed stream(s) that determines which phase(s) can disappear in the column. We illustrate this for the original Case Study 1 in Figure 18, which

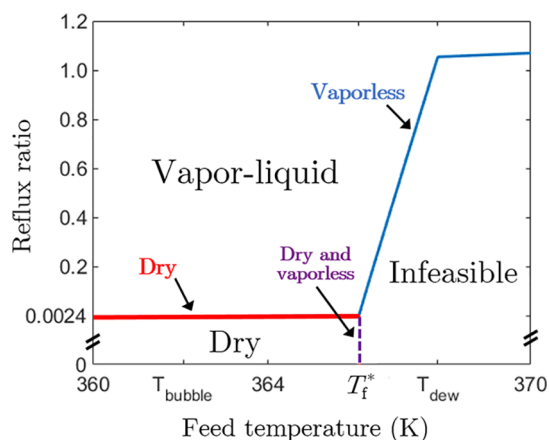


Figure 18. Critical reflux ratio R_{cr} versus feed temperature T_f for Case Study 1, with phase regimes for each (T_f, R) pair.

shows how R_{cr} changes as we vary the feed temperature, and the corresponding phase regimes at, above, or below the critical reflux curve. A change in regimes occurs at the feed temperature $T_f^* = 366.07$ K, which is between the bubble and dew-point temperatures $T_{bubble} = 362.0$ K and $T_{dew} = 367.9$ K of the feed mixture. For feed temperatures below T_f^* , the column goes dry above the feed stage for $R \leq R_{cr}$, starting with $L_5 = 0$, in the same fashion depicted in Figure 9. For higher feed temperatures, the column becomes vaporless below the feed stage at $R = R_{cr}$ in the same fashion of Figure 14, starting with $V_7 = 0$, and smaller reflux ratios $R < R_{cr}$ are infeasible.

However, exactly at the transitional feed temperature T_f^* , the column becomes simultaneously dry above the feed and vaporless below the feed for $R \leq R_{cr}$, starting with $L_5 = V_7 = 0$. In this case, any of the infinitely many vaporless states of the below-feed part of the column can occur simultaneously with

any dry state of the above-feed section corresponding to $0 < R \leq R_{cr}$. As a result, we arrive at another type of nonsmooth bifurcation with a higher degree of degeneracy. The main aspects of this complex behavior can be illustrated by Figure 19, where L_4 (representing above-feed states) and V_8

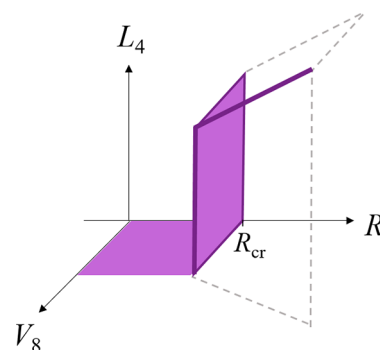


Figure 19. The codimension-2 bifurcation at $T_f = T_f^*$, in terms of L_4 and V_8 versus R .

(representing below-feed states) are plotted against R at $T_f = T_f^*$. At $R = R_{cr}$, the solution set is a 2-dimensional PC^r manifold of steady states instead of a 1-dimensional PC^r manifold. For each individual reflux ratio $0 \leq R < R_{cr}$, there are infinitely many vaporless steady states forming a 1-dimensional PC^r manifold, whereas the overall solution set for $0 \leq R \leq R_{cr}$ is a 2-dimensional PC^r manifold containing dry and vaporless steady states.

While all other bifurcations presented in this paper have codimension 1 and thus require only a single parameter to be varied, the bifurcation at $R = R_{cr}$, $T_f = T_f^*$ is of codimension 2: two parameters are involved simultaneously, the reflux ratio and the feed temperature. Therefore, it is much less likely to be observed in practice during simulation of the nonsmooth MESH model.

Figure 20 presents the phase regimes in terms of the boilup ratio versus T_f for the same system, and we see a qualitatively

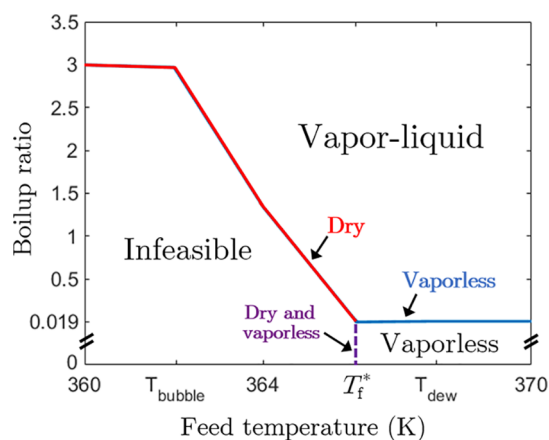


Figure 20. Critical boilup ratio B_{cr} versus feed temperature T_f for Case Study 1, with phase regimes for each (T_f, B) pair.

analogous behavior. We can also conclude from Figures 18 and 20 that the magnitude of the critical parameter value is not necessarily small and depends on several factors. As a result, engineers or solution algorithms could inadvertently choose input parameters close to or below their critical values during

column simulation and optimization, leading to failure of any current MESH-based software.

Multiple Feeds. When multiple feeds are present, the location and phase (vapor/liquid) of the first vanishing stream is not obvious and cannot be predicted prior to simulation, but is usually directly above or below one of the feed stages since flow rates tend to vary monotonically in each column section.

To exemplify the different types of behavior that can be observed, consider the original Case Study 1 with a bubble-point liquid fed into Stage 6. If we introduce a second liquid feed stream into a stage above, say, Stage 4, then the same type of bifurcation from Figure 9 now happens above this second feed only, with Stages 2–3 becoming dry. If instead we introduce a second vapor feed below Stage 6, say, at Stage 8, the type of bifurcation observed at R_{cr} might change according to the behavior in Figure 18, with the horizontal axis now representing the vapor feed flow rate F_8 . That is, for large enough values of F_8 , the column is vaporless below Stage 8 at $R = R_{cr}$, and for small enough F_8 values, it remains dry above Stage 6 for $R \leq R_{cr}$. At a transitional vapor feed flow rate F_8^* , the column is simultaneously dry above Stage 6 and vaporless below Stage 8 for $R \leq R_{cr}$.

The Type of Condenser and the Bifurcation at $R = 0$.

The nonsmooth bifurcation that occurs at $R = 0$ in a column with dry stages depends on the type of condenser specified. As long as the vapor distillate fraction θ is smaller than 1, a non-zero amount of liquid distillate W_{L1} is present and the condenser never goes dry. As a result, the solution curve stops at $R = 0$ and we observe the same $0 - 1 - 1$ bifurcation described in the original Case Study 1.

However, if $\theta = 1$, the condenser becomes dry at $R = 0$ and the outlet vapor V_1 can become superheated, which is associated with a positive condenser heat duty Q_1 . The solution curve is allowed to continue varying at $R = 0$ as the condenser temperature T_1 progressively increases, and we observe a $0 - \infty - 1$ bifurcation, depicted in Figure 21 for Case Study 1. This bifurcation is analogous to that observed at $B = 0$ for the reboiler in a vaporless column, which is illustrated in Figure 15.

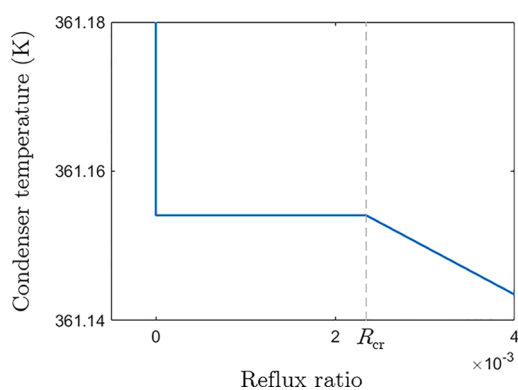


Figure 21. Condenser temperature T_1 versus R for Case Study 1 with $\theta = 1$.

Side Products. The type of bifurcations occurring at the critical parameter values might change when we withdraw side products from intermediate stages, depending on their phase (vapor/liquid) and location relative to the feed streams. We illustrate the possible behaviors with Case Study 1, in which a liquid feed is introduced into Stage 6. If a vapor side product is

included anywhere in the column or if a liquid side product is withdrawn from a stage below the feed, the types of bifurcations previously presented remain the same. However, the system behavior changes if we include a liquid side product above the feed, depending on the type of specification chosen and stage location.

Withdrawal Ratio Specification. If we specify a liquid withdrawal ratio $R_{L,j}$ for an intermediate stage j above the feed, the stage's drying process can proceed normally due to eq 28 but is no longer degenerate, as illustrated in Figure 22a for Stage 3 with $R_{L,3} = 0.5$. At the new critical reflux ratio value $R_{cr} \approx 0.0030$, we observe infinitely many solutions due solely to the drying process of Stage 4. The drying process of Stage 3 happens with a unique solution for each R , until we reach a second reflux ratio value $R^* = 0.0024$ with infinitely many solutions corresponding to the drying process for Stage 2. Therefore, two $1 - \infty - 1$ bifurcations happen in series: at R_{cr} and R^* . Taking a step further, if we specify the same liquid withdrawal ratio $R_{L,j} = 0.5$ for Stages 2, 3, and 4, we can eliminate the occurrence of infinitely many solutions and the corresponding bifurcations altogether, as shown in Figure 22b.

Flow Rate Specification. When we specify a liquid side product flow rate $W_{L,j}$ in stage j above the feed, the stage can never become dry. If the stage's liquid outlet L_j reaches zero, its corresponding mid equation (eq 23) does not switch between its arguments and remains enforcing the summation relationship. Once $L_j = 0$ in the continuation process, the only way to continue tracing solutions would be with $L_j < 0$, which is not allowed by eq 29. Therefore, the nonsmooth MESH model ceases to have a solution, which is illustrated in Figure 23a for Case Study 1 with $W_{L,5} = 0.1$ mol/s. Stage 5, directly above the feed, goes dry at $R_{cr} \approx 0.00446$ and the solution curve cannot proceed any further, with a $0 - 1 - 1$ bifurcation observed at R_{cr} . On the other hand, if we specify a liquid side product flow rate $W_{L,2} = 0.1$ mol/s in Stage 2, the drying process of Stages 3 and 4 is allowed to happen in the original degenerate fashion, as depicted in Figure 23b. This originates infinitely many solutions at $R_{cr} = 0.00445$; however, the solution curve stops once the outlet liquid L_2 reaches zero, and we obtain a $0 - / \infty - 1$ bifurcation at R_{cr} .

SUMMARY OF BIFURCATIONS

Table 1 presents all codimension-1 bifurcations introduced in this paper in their simplest or normal form, which corresponds to the bifurcation at $\lambda = 0$ of a simple single-equation, single-variable system $f(x, \lambda) = 0$ with the same essential behavior. In all instances, the overall solution set is a connected 1-dimensional PC^r manifold, with or without boundary; moreover, the three first bifurcations depicted in Table 1 are degenerate. Finally, we draw attention to the possibility that other combinations of column specifications not considered in this paper could give rise to other types of novel, nonsmooth bifurcations in dry/vaporless distillation columns.

CONCLUSIONS AND FUTURE WORK

We have presented a MESH-based steady-state model for multistage distillation, consisting of a system of nonsmooth equations, that can simulate columns operating with dry and/or vaporless stages. This task cannot be achieved with commercial software such as Aspen Plus, which has well-known dry column simulation failures, since the describing equations for each stage need to be automatically switched

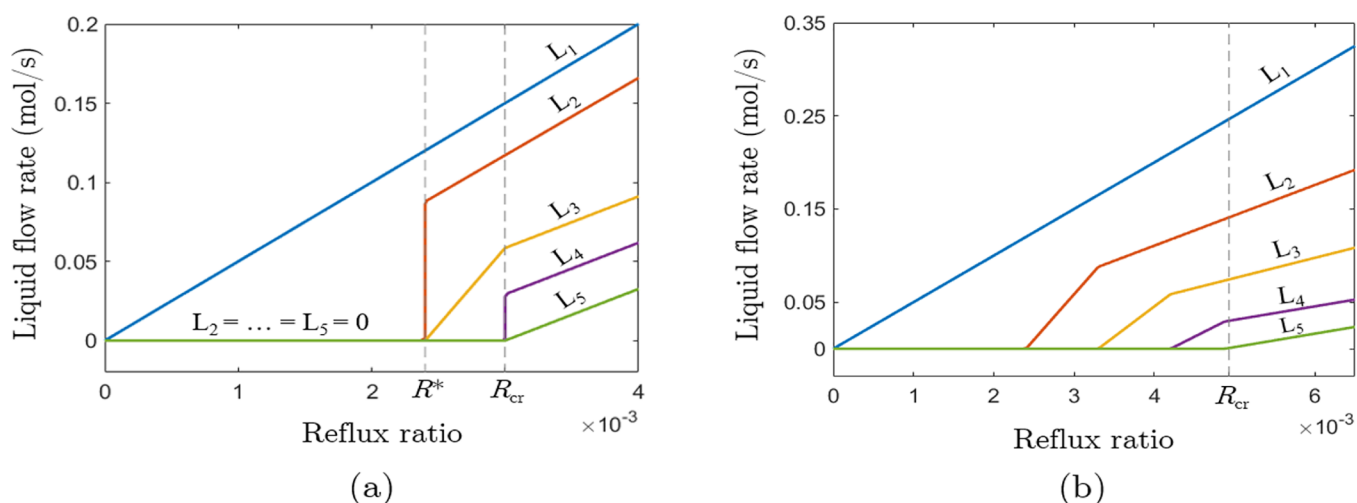


Figure 22. Above-feed liquid flow rates versus R for Case Study 1 with (a) $R_{L,3} = 0.5$ and (b) $R_{L,j} = 0.5, j = 2,3,4$.

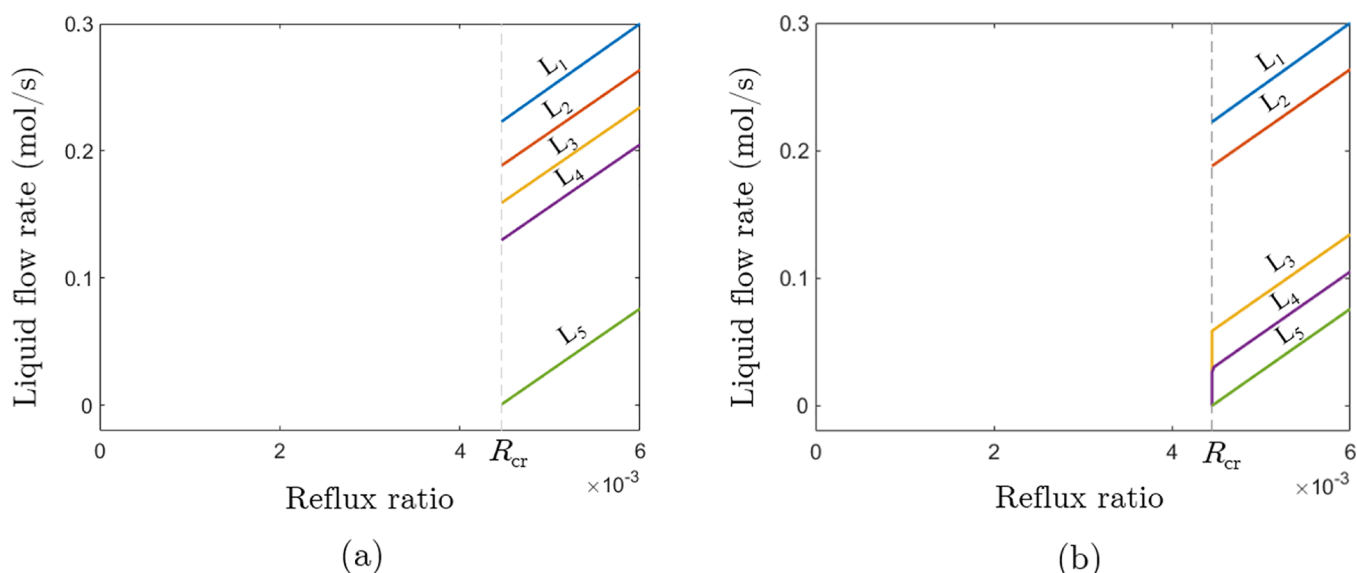


Figure 23. Above-feed liquid flow rates versus R for Case Study 1 with (a) $W_{L,5} = 0.1$ mol/s and (b) $W_{L,2} = 0.1$ mol/s.

according to the phases present at the solution. The only other competing modeling strategy in the literature relies on complementarity constraints, which require several equation-solving tasks or the use of optimization algorithms. On the other hand, our model can be solved in a single equation-solving task using automatically computed generalized derivatives, and can bound flow rates and other variables to be non-negative. Moreover, the algebraic nature of our model has allowed us to develop the necessary continuation methods to reveal, for the first time, the occurrence of an infinite number of steady states in distillation columns with dry and/or vaporless stages.

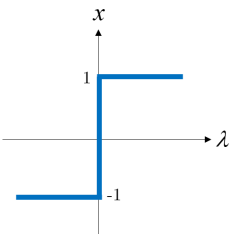
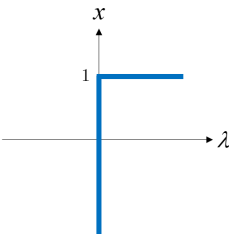
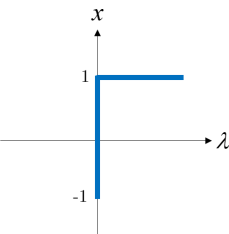
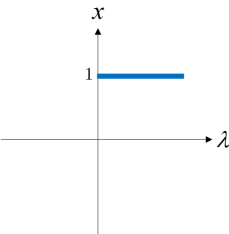
In two case studies involving dry/vaporless distillation columns from the pertinent literature, we have observed four novel types of codimension-1 bifurcations, classified according to the change in the number of steady states with respect to a single input parameter: $1 - \infty - 1$, $0 - \infty - 1$, and $0 - / \infty - 1$ (degenerate) and $0 - 1 - 1$ (non-degenerate). By further analyzing several types of column configurations, we demonstrate that degenerate bifurcations occur at critical input parameter values in a general context, regardless of the

mixture and thermodynamic models, as long as there is either a pressure gradient in the column or imposed heat transfer in the trays. The degeneracy persists even when non-ideal stage efficiencies of different types are specified and when multiple feed streams and side products are included. We have also found that a codimension-2 bifurcation with a higher degree of degeneracy can occur when two input parameters are varied simultaneously. All presented bifurcations exhibit nonsmooth behavior, mathematically described by the proposed concept of piecewise-smooth manifolds.

Our findings further demonstrate that the input parameter values leading to dry/vaporless stages in a distillation column are not necessarily small, cannot be predicted prior to simulation, and often give rise to an infinite number of steady states. This degeneracy is associated with singular generalized derivatives; therefore, it requires special continuation methods that are not currently implemented in general process flowsheeting software. Moreover, in some cases, no feasible solutions exist below the critical parameter values.

In the subsequent work, we will focus on developing alternative nonsmooth formulations to address both the

Table 1. Summary of Codimension-1 Bifurcations

Bifurcation	1 - ∞ - 1	0 - ∞ - 1	0 - /∞ - 1	0 - 1 - 1
Normal form $f(x, \lambda) = 0$	 $\text{mid}(x+1, -\lambda, x-1) = 0$	 $\text{max}(x-1, -\lambda) = 0$	 $\text{min}(x+1, - \text{max}(x-1, -\lambda)) = 0$	 $\text{min}(\lambda, - x-1) = 0$
Solution set around $\lambda = 0$	1-dimensional PC^r manifold	1-dimensional PC^r manifold	1-dimensional PC^r manifold w/ 1 boundary point	1-dimensional PC^r manifold w/ 1 boundary point
Solution set at $\lambda = 0$	1-dimensional PC^r manifold w/ 2 boundary points	1-dimensional PC^r manifold w/ 1 boundary point	1-dimensional PC^r manifold w/ 2 boundary points	A single point (0-dimensional PC^r manifold)
Examples	- Figures 9, 11 at $R = R_{cr}$; - Figure 14b at $B = B_{cr}$; - Figure 22a at $R = R_{cr}$ and $R = R^*$.	- Figure 15 at $B = 0$; - Figure 21 at $R = 0$.	- Figures 12, 13 at $B = B_{cr}$; - Figure 23b at $R = R_{cr}$.	- Figures 9, 11 at $R = 0$; - Figure 23a at $R = R_{cr}$.

singularity and infeasibility limitations, in order to create a distillation model that is robust to the issues associated with dry/vaporless stages and applicable for flowsheet simulation in industrial practice. Another line of future work involves the dynamic simulation of dry/vaporless distillation columns and stability analysis of the predicted infinitely many steady states, which could shed light on the possibility of observing this degenerate behavior in an experimental setting. Finally, we note that our nonsmooth modeling and continuation strategies could be extended to analyze phase regime transitions in vapor–liquid–liquid systems. Previous computational and experimental results on heterogeneous azeotropic distillation^{36,37} seem to indicate a discontinuity in steady states associated with the appearance of a second liquid phase in several stages, which could suggest the occurrence of degenerate bifurcations analogous to the ones we presented in this paper.

AUTHOR INFORMATION

Corresponding Author

Paul I. Barton – Massachusetts Institute of Technology, Process Systems Engineering Laboratory, Cambridge, Massachusetts 02139, United States; orcid.org/0000-0003-2895-9443;
Email: pib@mit.edu

Author

Suzane M. Cavalcanti – Massachusetts Institute of Technology, Process Systems Engineering Laboratory, Cambridge, Massachusetts 02139, United States; orcid.org/0000-0003-0020-6255

Complete contact information is available at:
<https://pubs.acs.org/10.1021/acs.iecr.0c02328>

Notes

The authors declare no competing financial interest.

ACKNOWLEDGMENTS

This publication has been funded by HighEFF – Centre for an Energy Efficient and Competitive Industry for the Future. The authors gratefully acknowledge the financial support from the Research Council of Norway and user partners of HighEFF, an 8 year Research Center under the FME-scheme (Centre for Environment-friendly Energy Research, 257632).

REFERENCES

- (1) Humphrey, J. L.; Keller, G. E., II *Separation Process Technology*; McGraw-Hill: New York, NY, 1997.
- (2) *Materials for Separation Technologies: Energy and Emission Reduction Opportunities*; Oak Ridge National Laboratory: Oak Ridge, TN, 2005.
- (3) Seader, J. D.; Henley, E. J.; Roper, D. K. *Separation Process Principles*; 3rd ed.; John Wiley & Sons, Inc.: Hoboken, NJ, 2011.
- (4) Krishnamurthy, R.; Taylor, R. A nonequilibrium stage model of multicomponent separation processes. Part I: Model description and method of solution. *AIChE J.* **1985**, *31*, 449–456.
- (5) Taylor, R.; Krishna, R.; Koojiman, H. Real-World Modeling of Distillation. *Chem. Eng. Prog.* **2003**, *99*, 28–39.
- (6) *Aspen Plus V10*; Aspen Technology Inc.: Bedford, MA, 2017.
- (7) Bullard, L. G.; Biegler, L. T. Iterated linear programming strategies for non-smooth simulation: a penalty based method for vapor-liquid equilibrium applications. *Comput. Chem. Eng.* **1993**, *17*, 95–109.
- (8) Gopal, V.; Biegler, L. T. Smoothing Methods for Complementarity Problems in Process Engineering. *AIChE J.* **1999**, *45*, 1535–1547.
- (9) Lang, Y.-D.; Biegler, L. T. Distributed Stream Method for Tray Optimization. *AIChE J.* **2002**, *48*, S82–S95.
- (10) Raghunathan, A. U.; Biegler, L. T. Mathematical programs with equilibrium constraints (MPECs) in process engineering. *Comput. Chem. Eng.* **2003**, *27*, 1381–1392.
- (11) Raghunathan, A. U.; Diaz, M. S.; Biegler, L. T. An MPEC formulation for dynamic optimization of distillation operations. *Comput. Chem. Eng.* **2004**, *28*, 2037–2052.
- (12) Dowling, A. W.; Biegler, L. T. A framework for efficient large scale equation-oriented flowsheet optimization. *Comput. Chem. Eng.* **2015**, *72*, 3–20.

- (13) Dowling, A. W.; Balwani, C.; Gao, Q.; Biegler, L. T. Equation-Oriented Optimization of Cryogenic Systems for Coal Oxy-combustion Power Generation. *Energy Procedia* **2014**, *63*, 421–430.
- (14) Zhu, D.; Eason, J. P.; Biegler, L. T. Energy-efficient CO₂ liquefaction for oxycombustion power plant with ASU-CPU integration enhanced by cascaded sub-ambient energy utilization and waste heat recovery. *Int. J. Greenhouse Gas Control* **2017**, *61*, 124–137.
- (15) Khan, K. A.; Barton, P. I. A vector forward mode of automatic differentiation for generalized derivative evaluation. *Optim. Methods Software* **2015**, *30*, 1185–1212.
- (16) Watson, H. A. J.; Barton, P. I. Modeling phase changes in multistream heat exchangers. *Int. J. Heat Mass Transfer* **2017**, *105*, 207–219.
- (17) Watson, H. A. J.; Vikse, M.; Gundersen, T.; Barton, P. I. Reliable flash calculations: Part 1. Nonsmooth inside-out algorithms. *Ind. Eng. Chem. Res.* **2017**, *56*, 960–973.
- (18) Sahlodin, A. M.; Watson, H. A. J.; Barton, P. I. Nonsmooth Model for Dynamic Simulation of Phase Changes. *AIChE J.* **2016**, *62*, 3334–3351.
- (19) Keller, H. B. *Recent Advances in Numerical Analysis: Proceedings of a Symposium Conducted by the Mathematics Research Center at the University of Wisconsin-Madison, May 22–24, 1978*; Academic Press: New York, NY, 1978; pp 73–94.
- (20) Magnussen, T.; Michelsen, M. L.; Fredenslund, A. Azeotropic Distillation Using UNIFAC. *Inst. Chem. Eng. Symp. Ser.* **1979**, *56*, 4.2/1–4.2/19.
- (21) Bekiaris, N.; Meski, G. A.; Radu, C. M.; Morari, M. Multiple Steady States in Homogeneous Azeotropic Distillation. *Ind. Eng. Chem. Res.* **1993**, *32*, 2023–2038.
- (22) Lee, M.; Dorn, C.; Meski, G. A.; Morari, M. Limit cycles in homogeneous azeotropic distillation. *Ind. Eng. Chem. Res.* **1999**, *38*, 2021–2027.
- (23) Jacobsen, E. W.; Skogestad, S. Multiple Steady States in Ideal Two-Product Distillation. *AIChE J.* **1991**, *37*, 499–511.
- (24) Carranza-Abaid, A.; González-García, R. A Petlyuk distillation column dynamic analysis: Hysteresis and bifurcations. *Chem. Eng. Process.* **2020**, *149*, 107843.
- (25) Kovach, J. W., III; Seider, W. D. Heterogeneous Azeotropic Distillation-Homotopy-Continuation Methods. *Comput. Chem. Eng.* **1987**, *11*, 593–605.
- (26) Kienle, A.; Groebel, M.; Gilles, E. D. Multiple Steady States in Binary Distillation - Theoretical and Experimental Results. *Chem. Eng. Sci.* **1995**, *50*, 2691–2703.
- (27) Müller, D.; Marquardt, W. Experimental Verification of Multiple Steady States in Heterogeneous Azeotropic Distillation. *Ind. Eng. Chem. Res.* **1997**, *36*, 5410–5418.
- (28) Bekiaris, N.; Güttinger, T. E.; Morari, M. Multiple Steady states in Distillation: Effect of VL(L)E Inaccuracies. *AIChE J.* **2000**, *46*, 955–979.
- (29) Grossmann, I. E.; Trespacios, F. Systematic modeling of discrete-continuous optimization models through generalized disjunctive programming. *AIChE J.* **2013**, *59*, 3276–3295.
- (30) Watson, H. A. J.; Khan, K. A.; Barton, P. I. Multistream heat exchanger modeling and design. *AIChE J.* **2015**, *61*, 3390–3403.
- (31) Watson, H. A. J.; Vikse, M.; Gundersen, T.; Barton, P. I. Reliable flash calculations: Part 2. Process flowsheeting with nonsmooth models and generalized derivatives. *Ind. Eng. Chem. Res.* **2017**, *56*, 14848–14864.
- (32) Scholtes, S. *Introduction to Piecewise Differentiable Equations*; Springer: New York, NY, 2012, DOI: 10.1007/978-1-4614-4340-7.
- (33) Qi, L.; Sun, J. A nonsmooth version of Newton's method. *Math. Program.* **1993**, *58*, 353–367.
- (34) Facchinei, F.; Pang, J.-S. *Finite-Dimensional Variational Inequalities and Complementarity Problems*; Springer-Verlag New York, Inc.: New York, NY, 2003; Vol. 2.
- (35) Holland, C. D.; McMahon, K. S. Comparison of vaporization efficiencies with Murphree-type efficiencies in distillation-I. *Chem. Eng. Sci.* **1970**, *25*, 431–436.
- (36) Kovach, J. W., III; Seider, W. D. Heterogeneous Azeotropic Distillation: Experimental and Simulation Results. *AIChE J.* **1987**, *33*, 1300–1314.
- (37) Widagdo, S.; Seider, W. D.; Sebastian, D. H. Bifurcation Analysis in Heterogeneous Azeotropic Distillation. *AIChE J.* **1989**, *35*, 1457–1464.